Respiratory and Cardiac Motion Correction Using the Beat Pilot Tone

Katie Lamar
Michael Lustig, Ed.
Suma Anand, Ed.

Electrical Engineering and Computer Sciences
University of California, Berkeley

Technical Report No. UCB/EECS-2023-169
http://www2.eecs.berkeley.edu/Pubs/TechRpts/2023/EECS-2023-169.html

May 12, 2023

Acknowledgement

I would first and foremost like to thank my advisor, Dr. Michael (Miki) Lustig and my mentor, Suma Anand, for their unwavering support and guidance. I truly cannot find the words to express how honored and grateful I am to have had the opportunity to work with them both.

I would like to thank Dr.Chunlei Liu for all of the insights, suggestions, and knowledge he shared with me. I would also like to thank Ekin Karasan for all of her help with RTHawk, Spinbench, and cable trap design. I would like to extend my gratitude to Rebekah Zhao, Julian Maravilla, and Karthik Gopalan for all of the hardware-related help they provided. As well as to Shreya Ramachandran for helping me acquire 3D Fast SPGR images on a GE scanner and teaching me all there is to know about SENSE Reconstruction.

Respiratory and Cardiac Motion Correction Using the Beat Pilot Tone

by Katie Lamar

Research Project

Submitted to the Department of Electrical Engineering and Computer Sciences, University of California at Berkeley, in partial satisfaction of the requirements for the degree of **Master of Science, Plan II**.

Approval for the Report and Comprehensive Examination:

Committee:

Professor Michael Lustig
Research Advisor

05/12/2023

(Date)

* * * * * * *

Professor Chunlei Liu
Second Reader

05/11/2023

(Date)

Respiratory and Cardiac Motion Correction Using the Beat Pilot Tone

Thesis by
Katie Lamar

In partial fulfillment of the requirements for the Master of Science Degree in Electrical Engineering Computer Science

UNIVERSITY OF CALIFORNIA, BERKELEY
Berkeley, California

2022-2023

Kathryn Lamar
ORCID: 0000-0003-0708-1774

ACKNOWLEDGEMENTS

I would first and foremost like to thank my advisor, Dr. Michael (Miki) Lustig and my mentor, Suma Anand, for their unwavering support and guidance. As cheesy as it may sound, I truly cannot find the words to express how honored and grateful I am to have had the opportunity to work with them both. I have grown tremendously under their guidance and they have inspired me to remain curious and passionate about the research I pursue.

I would like to thank Dr.Chunlei Liu for all of the insights, suggestions, and knowledge he shared with me. He pushed me to dive deeper into MR pulse sequence design and I'm very excited to start focusing on this research area at UC San Diego.

I would also like to thank Ekin Karasan for all of her help with RTHawk, Spinbench, and cable trap design. I would like to extend my gratitude to Rebekah Zhao, Julian Maravilla, and Karthik Gopalan for all of the hardware-related help they provided. I would also like to thank Shreya Ramachandran for helping me acquire 3D Fast SPGR images on a GE scanner and teaching me all there is to know about SENSE Reconstruction. Lastly, I'd like to thank all of MikGroup and Professor Chunlei Liu's lab for all of the kindness and support they provided throughout this journey.

TABLE OF CONTENTS

LIST OF ILLUSTRATIONS

Number *Page*

ABSTRACT

Magnetic Resonance Imaging (MRI) is a noninvasive imaging modality that can provide high spatial resolution images of human anatomy in addition to rich dynamic and quantitative information without the need for ionizing radiation. Unfortunately, this high spatial resolution comes at the cost of very low temporal resolution, leaving adequate time for motion to corrupt one's images. Motion correction and prevention remains a main research focus in the MR community. In this work, we explore a motion tracking method that uses microwave frequencies, known as the Beat Pilot Tone (BPT), to detect a wide range of motion without the need for additional on-subject hardware and or changes to the MRI sequence. The BPT, unlike other RF tracking methods, has sensitivity and accuracy comparable to conventional motion tracking methods (e.g. respiratory bellows, electrocardiogram (ECG), photoplethysmogram (PPG)) [1][2][3].

In this work, we focus on demonstrating the effectiveness of the BPT at resolving motion in cardiac and abdominal images both retrospectively and prospectively. We show that the BPT provides highly sensitive and accurate motion estimates, resulting in retrospectively-corrected images comparable to the images corrected using the motion estimates provided by ECG and respiratory bellows. We also implemented a prospective free-breathing BPT navigated 3D SPGR application in Vista.ai's RTHawk MR Research Platform. We show that with minimal real-time processing techniques, we are able to attain images comparable to images provided by GE's respiratory bellows navigated 3D SPGR LAVA ASPIR sequence.

Chapter 1

INTRODUCTION

Medical professionals often rely on the essential anatomic and dynamic information provided by noninvasive, medical imaging modalities in order to diagnose, treat, and monitor patients. Although tremendous strides have been made to improve these modalities, limitations still persist. For example, ultrasound provides high temporal resolution images; however, it has poor contrast and low signal-to-noise ratio (SNR). Computed Tomography (CT) has high temporal and spatial resolution, but at the cost of poor contrast and exposure to ionizing radiation. Magnetic Resonance Imaging (MRI) is capable of providing high spatial resolution, excellent soft-tissue contrast, and high SNR without ionizing radiation. Unfortunately, high spatial resolution comes at the cost of low temporal resolution, allowing ample opportunity for motion of the subject or patient to corrupt MR images.

MR images can attain rich quantitative and dynamic information with high spatial resolution; however, these acquisitions are often hindered by motion artifacts. Motion correction for MRI is a very active research area that seeks to mitigate these artifacts. In particular, cardiac and respiratory motion continue to be the main culprits of low-quality, artifact-corrupted MR cardiac and abdominal images. An example of a motion-corrupted cardiac scan is shown in Figure 1.1. Because the MR image in Figure 1.1 was acquired over 1.1 seconds, cardiac motion caused blurring of the myocardial wall (indicated by the green arrows).

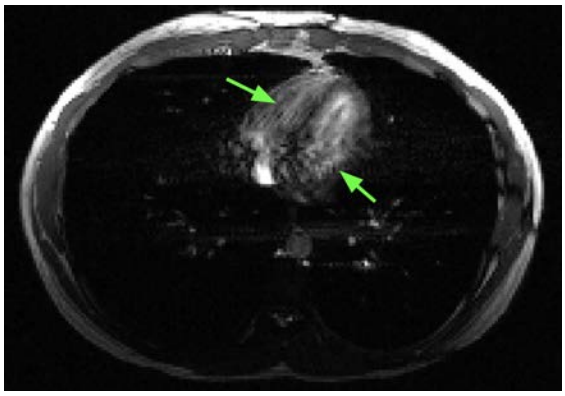

Figure 1.1: An MR image was acquired with a 2D balanced SSFP sequence on a healthy volunteer while they were holding their breath. Since the acquisition took 1.1 seconds, cardiac motion resulted in a blurred image (indicated by the green arrows).

The numerous motion correction methods that have been designed and implemented thus far attempt to provide accurate motion correction without creating additional limitations and/or safety risks. These methods can be sorted into the following categories listed in Table 1.1.

Main Types of Motion Reducing Methods	
Approach	**Examples**
Motion Suppression	Provide instructions, stabilize subject, sedation, pharmacological agents, etc.
Moving Tissue Signal Suppression	Spatial saturation pulses, fat suppression techniques,etc.
Motion Reducing Pulse Sequences & Parameters	Rapid sequences, Radial/Spiral acquisitions, increase NEX, etc.
Tracking-based Motion Compensation	On-subject hardware (e.g. ECG, PPG, Bellows), navigator, center of k-space oversampling, etc.

Table 1.1: Main Types of Motion Reducing Methods

Ideally, a motion sensing method should have three main desired characteristics: high motion sensitivity/accuracy, high subject comfort and safety, and MR scan independence [4]. The motion-alleviating approaches and the many examples provided for each approach mentioned in the previous table all have their own benefits; however, they are not able to satisfy all three qualities..

In our previous work, we proposed a microwave frequency-based motion sensing method known as the Beat Pilot Tone (BPT) that can be used to track subject motion

throughout an MR exam. It does so with high motion sensitivity and accuracy, ensures subject comfort and safety, and is independent of the MRI scan or "pulse sequence" [1][2][5]. The focus of this work is to demonstrate that BPT-based correction for cardiac and respiratory motion yields images that have comparable quality to images attained using other tracking methods, which may require hardware placed on the subject or changes to the pulse sequence. We demonstrate both prospective and retrospective motion correction. Additionally, the hardware setup can be easily integrated into any MR system at a low cost.

We begin by first providing the necessary MR physics background to understand how MR images are acquired and processed (chapter 2). In chapter 3, the BPT mechanism is formally introduced along with other radio frequency (RF) motion tracking methods. The BPT hardware setup and safety measures taken are described in chapter 4. Retrospective motion correction methods and subsequent results are described in chapter 5. The real-time BPT processing methods are described in detail in chapter 6 and the software implementation of a BPT-Navigated, Free-Breathing 3D Spoiled Gradient Echo (SPGR) pulse sequence and the subsequent results can be found in chapter 7. Lastly, we summarize our work and discuss next steps in chapter 8. All experiments were performed on our GE 3T 750W MRI scanner.

Chapter 2

PRELIMINARIES

Magnetic Resonance Imaging (MRI) is an excellent imaging modality that provides high spatial resolution without the need for ionizing radiation and is capable of providing rich dynamic and quantitative information. The high spatial resolution, however, comes at the cost of temporal resolution; thus, motion correction methods are a necessity in order to utilize the full potential of MR imaging. In order to understand the BPT mechanism and its role in the MR environment, one must first be acquainted with basic MR physics.

2.1 Introducing NMR

MRI scanners exploit the phenomenon of Nuclear Magnetic Resonance (NMR), which describes how nuclei react when placed in a strong static magnetic field that is then perturbed by a weak, oscillating magnetic field.

Atoms that have an odd number of protons and/or neutrons possess a net **nuclear spin**. These atoms are not actually spinning; however, they do have **spin angular momentum**. In this chapter, we will refer to collections of atoms with a net nuclear spin as "spins".

Definition 1: Spin Angular Momentum

Spin Angular Momentum, **S**, is the vector quantity defined as follows:

$$\mathbf{S} = \frac{\hbar}{2\pi}\mathbf{I}$$

where $\hbar$ is Planck's Constant and **I** is the spin operator.

In order to fully understand the NMR phenomenon, one must dive deep into the area of quantum mechanics. Luckily, one can gain enough familiarity with the NMR concept as it relates to MRI by merely investigating the behavior of the popular children's toy, a spinning top.

One can motivate their spinning top investigation with a few key questions:

- *How does a spinning top prevent itself from falling over?*
- *How does a spinning top relate to MRI?*

How does a spinning top prevent itself from falling over?
Suppose you were to place the top directly on a flat surface (near the surface of the earth) without spinning it. Upon release, the top would fall over due to gravity applying a torque to the top's center of mass. If the top is instead spinning on its axis, there is no net torque acting on the top. Thus, the angular momentum's magnitude is constant, but the direction does change, leading to the top's precession about its axis.

How does a spinning top relate to MRI?
In the MR environment, ensembles of protons or spins can be considered as having a magnetic dipole moment. In order to understand this phenomenon, consider a charged particle spinning about its axis. This spin naturally gives rise to a loop of current, resulting in a magnetic dipole moment. This description is classical and does not describe what is actually occurring; however, the classical physics perspective provides a correct intuition regarding how these atoms behave in an MR environment.

Definition 2: Magnetic Dipole Momentum

The magnetic dipole moment, $\boldsymbol{\mu}$, is the vector quantity defined as follows:

$$\boldsymbol{\mu} = \gamma \mathbf{S} = \gamma \frac{\hbar}{2\pi} \mathbf{I}$$

where $\hbar$ is Planck's Constant, $\mathbf{I}$ is the spin operator, and γ is the gyromagnetic ratio which varies by atomic species.

Once placed in a magnetic field, an atom with a net nuclear spin will begin to precess about the magnetic field much like the spinning top precesses about its axis of rotation. The frequency of the precession is known as the **Larmor Frequency**.

Definition 3: Larmor Frequency

The processional frequency of an atom with *nuclear spin* $\neq 0$ in a time-constant magnetic field B is

$$\omega = \gamma |B|$$

where γ = gyromagnetic ratio of said atom.

The most abundant atomic species in the human body with a net nuclear spin is hydrogen, and MR imaging essentially measures the nuclear spin behavior of hydrogen protons as additional electromagnetic fields are applied.

2.2 How Does MR Imaging Actually Work?

Modern MRI scanners consist of three main components: a superconducting magnet, radiofrequency (RF) transmit and receive coils, and gradient coils. For simplicity, let us consider what happens when only hydrogen protons are placed in the MR environment. First, each proton aligns with the strong, static magnetic field, known as $\mathbf{B_0}$, and begins precessing about $\mathbf{B_0}$ at the Larmor Frequency as shown in Figure 2.1.

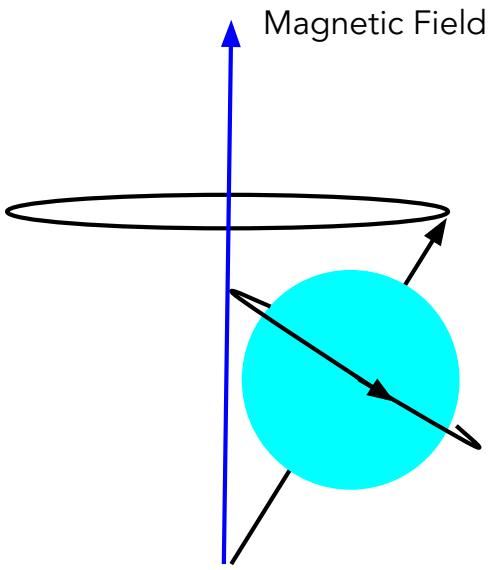

Figure 2.1: Protons can be thought of in analogy to spinning tops. They precess about an applied magnetic field $\mathbf{B_0}$ at a frequency proportional to its magnitude, known as the Larmor frequency [6]. Figure provided by [2].

One can imagine each proton as being a tiny bar magnet. When placed in a strong magnetic field, a bar magnet's poles will line up with the poles of the main magnetic field.

The magnetic moments of the protons will align with the magnetic field, but the direction (i.e. parallel vs. anti-parallel) of the alignment can vary. The magnetic dipole of a proton in the low energy state is aligned with the magnetic field direction, whereas the magnetic dipole of a proton in the high energy state is aligned in the opposite direction of the magnetic field. Naturally, most protons will remain in the low energy state and only a few will be in the high energy state as depicted in Figure 2.2. **Note:** traditionally the direction of the magnetic field (through the scanner's bore) is denoted as the z-axis.

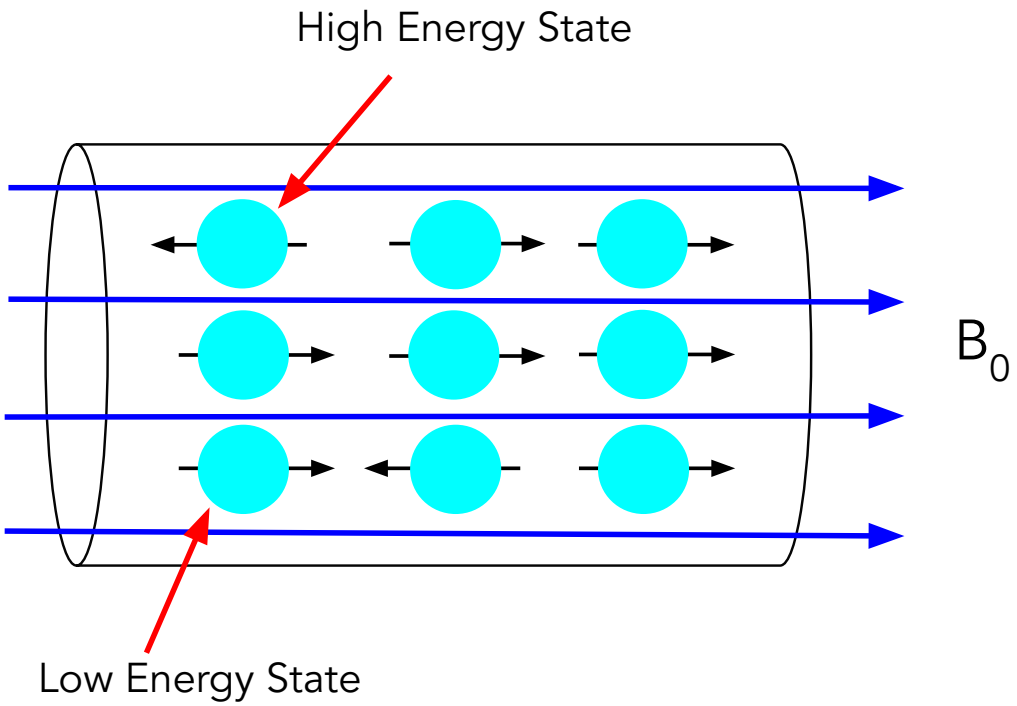

Figure 2.2: Protons tend to align with the magnetic field in a parallel (low energy state) or anti-parallel (high energy state) direction. More protons remain in the low energy state, and this net alignment is detected as a net magnetization [6]. Figure provided by [2].

The MRI scanner also has RF transmit and receive coils. The transmit coils are used to transmit an electromagnetic field $\mathbf{B_1}$ in the transverse direction at the Larmor frequency in order to "excite" the spins. From the classical physics perspective, this excitation is merely applying torque on the net magnetization, $\mathbf{M}$, which causes $\mathbf{M}$ to

rotate away from its equilibrium position along the z-axis while still precessing about the z-axis. This process results in the magnetization vector having a transverse (x-y) component in addition to a longitudinal (z) component. The transverse component of the magnetization is what is detected.

Definition 4: Net Magnetization

The net magnetization is defined as the sum of all the magnetic moments.

$$\mathbf{M} = \sum_i \boldsymbol{\mu}_i$$

where $\boldsymbol{\mu}_i$ is the ith proton's magnetic moment vector.

The $\mathbf{B_1}$ field is only applied for a short period of time. When the $\mathbf{B_1}$ pulse is turned off, the spins begin to return to their equilibrium, a process known as **relaxation**. Spins relax at different rates depending on the surrounding environment. This phenomenon is what can give rise to the excellent tissue contrast that MRI provides.

2.3 Acquiring MR Images

The RF receiver coils detect the transverse component of the net magnetization by exploiting Faraday's Law of Induction.

Theorem 1: Faraday's Law

The rate of change of the magnetic flux, Φ, through a loop with N turns is proportional to the induced voltage ϵ in the loop.

$$\epsilon = -N\frac{d\Phi}{dt}$$

Once the $\mathbf{B_1}$ pulse is applied, the net magnetization is knocked over, resulting in a change in flux through the coil elements (Figure 2.3). The change in flux induces an electromotive force (EMF) in the coil, denoted as $s(t)$ in Figure 2.3, which is the signal detected by the receiver coil over time. Immediately after the excitation, the transverse component of the magnetization begins to decay, and the longitudinal component of the magnetization returns to its thermal equilibrium [6]. The signal being detected is induced by the net magnetization moment of all of the spins and therefore does not encode any spatial information. The final set of coils, known as the gradient coils, are used to generate an electromagnetic field that encodes the position of spins in the frequency and phase of the resulting signal.

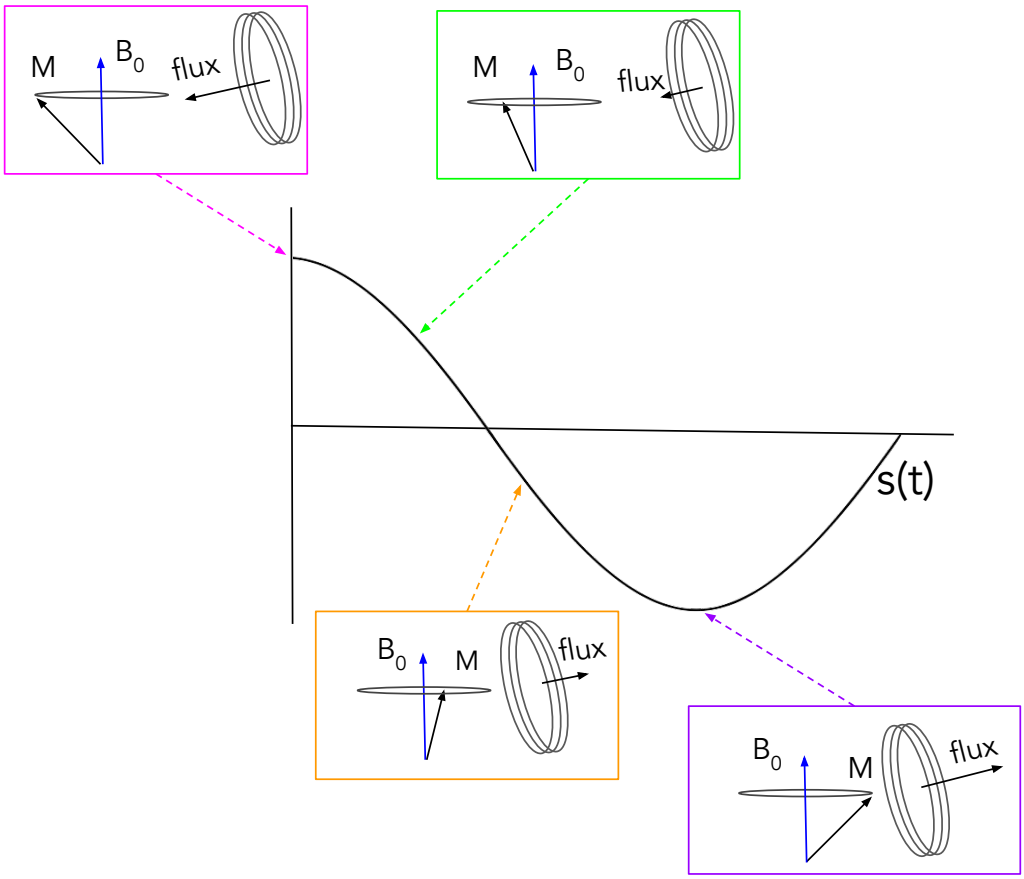

Figure 2.3: The relationship between the net magnetization and the MR signal acquired is shown above. As the net magnetization precesses, the flux changes through the coil and that rate of change is proportional to the EMF induced in the coil. Figure provided by [2].

The gradient coils are used to generate z-directed electromagnetic fields that vary linearly in the x, y, and z directions. We refer to these linearly-varying fields as "gradient fields" or simply "gradients". The gradients change the resonant frequency in these directions in order to encode the position of the magnetization in its frequency. An example of how the gradients vary the resonant frequency of the spins spatially is shown below.

Equation 1: Slice Select Gradient Example

Let the gradient in the z-direction be denoted as $G(z) = G_z z$ where G_z is a nonzero constant. The resonant frequency of spins at z_0 is as follows.

$$f(z_0) = \gamma(|\mathbf{B_0}| + G_z z_0)$$

In order to finally attain an image, we need to determine a relationship between the EMF signal induced in the coil and the anatomical images that the MR system is capable of providing; in other words, we need to reconstruct an image of the magnetization from the raw data. We give a 1D example of image reconstruction. As described in [6], if a gradient field is applied in one direction while the signal $s(t)$ is being acquired, the position of the spins along that direction is linearly proportional to the resonant frequency. Taking the inverse Fourier transform of $s(t)$ will yield a spectrum $S(f)$, which tells us how much energy is present at each frequency f. Since frequency is proportional to position, $|S(f)|$ is exactly the 1D image (or "projection") of the magnetization. Thus, the 1D image can be recovered by taking the inverse Fourier transform of the signal $s(t)$. The raw data $s(t)$ is also referred to as **k-space** data.

While we gave an example of 1-dimensional encoding, it is possible to acquire 2D or 3D data. In 2 dimensions, the k-space data is the 2D Fourier transform of the desired image [6]. One can therefore reconstruct this image by applying an inverse Fourier transform on the k-space data.

2.4 Receiver Coil Arrays

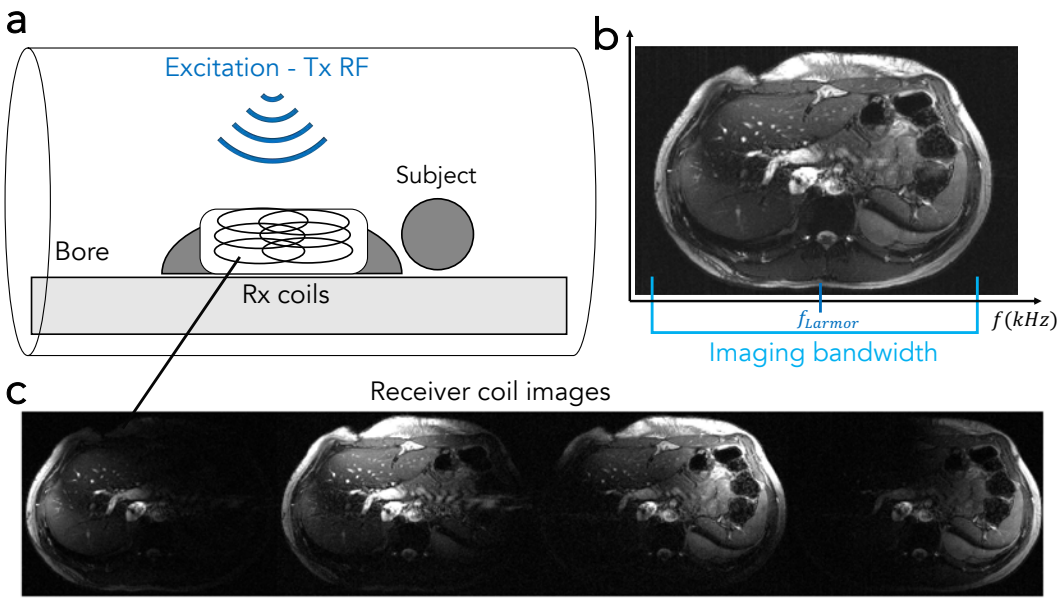

Figure 2.4: a) The setup of a typical MRI exam, in which the subject lies in the bore with an array of receiver coils placed on the imaging region (in this case, the abdomen). b) A sample MR image after combining the images from each coil. The image has a certain bandwidth, corresponding to the sampling rate of the receiver coils. c) The images from each receiver coil. Each coil is locally sensitive to a different region, providing additional spatial information in the MRI signal.

Instead of using just a single coil to detect the signal, an array of coils can be used to detect the MR signal simultaneously (Figure 2.4). An example of a receiver coil array placed on a subject is shown in Figure 2.3a. Each receiver coil is locally sensitive to the region around it (Figure 2.3c). The images from each coil can be combined to obtain a composite image with increased Signal-to-Noise Ratio (SNR) compared to a single coil image (Figure 2.3b). Moreover, each coil has an imaging bandwidth that it acquires, which is determined by the sampling rate set by the operator (Figure 2.3b). The anatomy occupies a portion of the bandwidth, but there is often extra space at the edges of the image that do not contain anatomical information. This is exploited by the Pilot Tone and Beat Pilot Tone motion sensing methods, which are discussed in chapter 3.

Coil-combining methods, described later in this work, were applied to attain coil-combined images and process motion estimates provided by information extracted from each coil.

Chapter 3

INTRODUCING THE BEAT PILOT TONE

RF motion tracking methods for MRI have been growing in popularity throughout the past decade due to the many advantages related to safety, comfort, and accuracy that these methods maintain [1][5][7][8][9][10][11][12]. RF motion tracking is capable of tracking a wide range of motion types, can provide motion sensitivity that is on par with conventional MR motion tracking methods, and doesn't require any additional on-subject hardware. There are many conventional and state-of-the-art motion tracking methods; however, here, we focus on commonly used methods such as navigators, electrocardiogram (ECG), photoplethysmogram (PPG), and respiratory bellows. Navigators are additional signals that are added into the acquisition which are generally NMR or MRI-based [13]. ECG, PPG, and respiratory bellows are motion sensors integrated into the MRI suite. They sense electrical signaling of the heart, optical changes in the skin based on blood pulsation, and changes in contraction of the abdomen due to breathing, respectively. RF-based methods at MHz frequencies mainly operate by sensing changes in the load impedance at the RF receiver or transmitter [14][15]. At clinical MRI field strengths, the dominant contribution to impedance comes from the human body. Subject motion then changes this impedance [14], leading to a change in the detected signal level. The resultant motion signal can be extracted and processed in order to attain motion estimates. RF methods that operate at higher frequencies, such as radar, could offer high quality multimodal information that is complementary to the MRI acquisition [7]. The many RF-based motion tracking and correcting methods that have been implemented thus far focus on increasing sensitivity, finding new ways to minimize the need for additional receiver systems (e.g. PT, BPT), and, of course, implementing robust motion correction methods using these motion estimates [1][5][7][8][9].

3.1 The Pilot Tone (PT)

The Pilot Tone (PT) is a RF-based motion tracking method that operates in the MHz range and takes advantage of the MR system's receiver chain, allowing one to collect the motion signal with the rest of the MR data [8][9]. The method consists of transmitting a single RF "Pilot" tone at a fixed frequency within the bandwidth of receiver throughout the MR exam [8][9]. The frequency should be chosen such

that the PT does not overlap with the anatomy of interest, but still lies within the bandwidth of the receiver such that the PT itself will be collected with the rest of the MR data. As described previously, the signal level of the PT is modulated by motion via changes in body impedance. The data is then extracted and processed for the purposes of prospective and retrospective motion correction, which will be described in-depth throughout this work. The PT, unlike radar motion tracking methods, does not need its own receiver chain, since it uses the MR system's receiver chain. The PT provides accurate bulk motion and respiratory estimates; however, to attain cardiac motion information, the PT antenna generally needs to be placed on the chest coil array [1][3]. Additionally, the signal attained does not provide detailed information about the cardiac motion cycle that sensors such as ECG have been shown to provide, which makes the PT navigator less ideal for cardiac triggering [16].

3.2 The Beat Pilot Tone (BPT)

The Beat Pilot Tone (BPT) aims at improving upon the PT navigator method while still utilizing the MR system's receiver chain. The BPT motion tracking method consists of transmitting two microwave frequency tones, which have been shown to be more sensitive to cardiac and other types of motion compared to the PT [1][3][7]. The frequency of the tones are fixed throughout the entirety of the scan and, similarly to the PT, the subject's motion modulates the signal. We choose the frequencies of the two tones, f_1 and f_2, such that the frequency difference of these tones ($f_2 - f_1$) is within the bandwidth of the receiver. Due to the non-linearity of the pre-amplifier in the receiver chain, the first order intermodulation product at frequency $f_{BPT} = f_2 - f_1$ is collected with the rest of the MR data, as shown in Figure 3.1. The BPT has been shown, in this work and in our past work, to be more sensitive to subject motion compared to the PT and could possibly provide information comparable to ECG [1][3][5]. In this thesis, we explore the application of the BPT to prospective and retrospective motion correction methods.

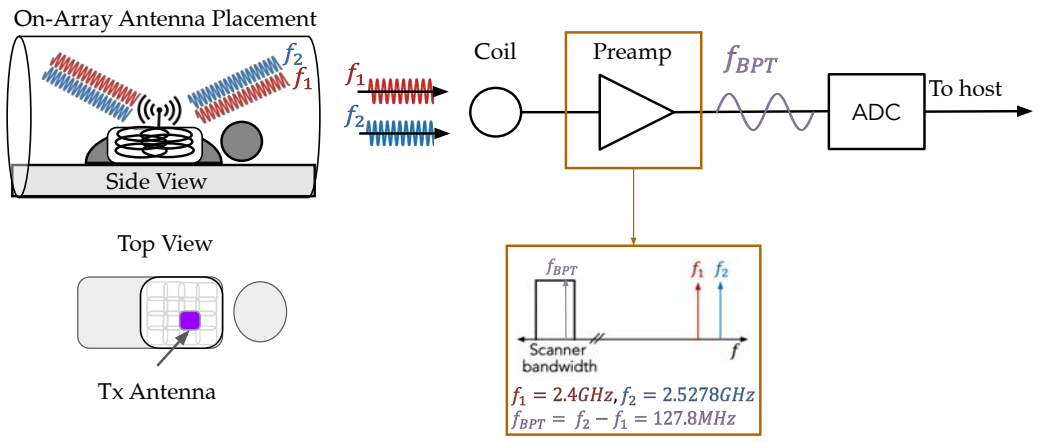

Figure 3.1: The BPT motion tracking method consists of transmitting two fixed-frequency tones at frequencies f_1 and f_2, which are separated by the MR bandwidth. These tones are then mixed in the preamplification stage via intermodulation to create a beat frequency. The beat frequency is digitized by the receiver chain and brought in with the rest of the MR data [1]. In this example, the Larmor frequency of the MRI scanner is $127.7MHz$.

3.3 Extracting the BPT/PT

The BPT and PT can both be extracted from the rest of the MR data using the same method. The BPT/PT signal, after applying a Fourier Transform along the readout direction of the MR data, will appear as a peak in the spectrum that can be easily separated from the rest of the MR data using the method shown in Figure 3.2. Once the BPT/PT signal is attained for each coil, it may be useful to combine the information across multiple coils or choose the most salient coil in order to obtain a 1D output signal often needed by certain retrospective or prospective motion correction techniques. In the motion correction methods found in this work, we either apply Principle Component Analysis (PCA) or choose the signal from the coil with the most energy in the frequency range of the motion being tracked. The types of processing methods applied to the motion signal are very dependent on the types of motion that one would like to track and are described in more detail later in this work.

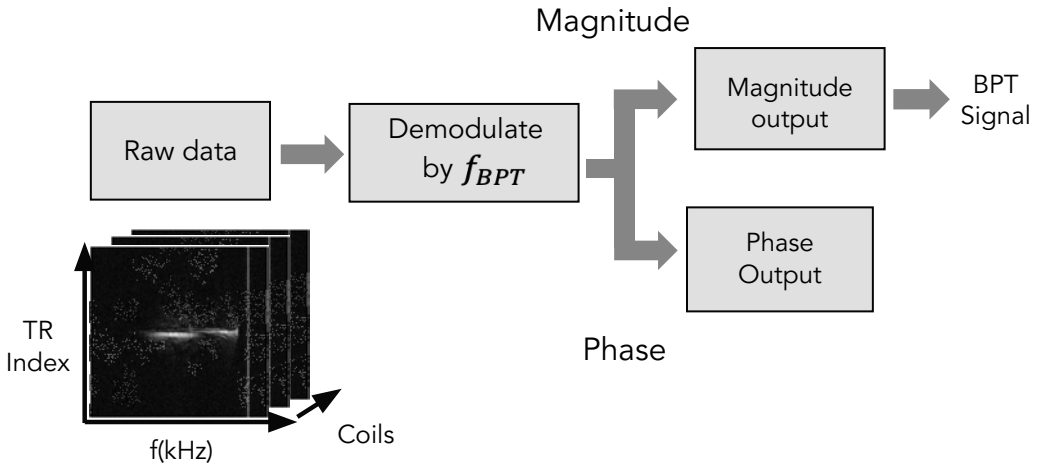

Figure 3.2: The BPT and PT signals were extracted by taking a 1D Fourier transform along the readout direction and selecting the points at the peak corresponding to the BPT frequency [5]. We used the extracted signal magnitude as our BPT signal for this work. The BPT's phase has rich motion information as well and in future work, we plan to incorporated this information into our motion correction method.

Chapter 4

BPT HARDWARE

The BPT and PT hardware setup can be easily integrated into any MR imaging system for a relatively low cost and without the need for any type of permanent hardware installation. The low cost and the portable setup make this motion tracking method accessible for both research and clinical use. In this section, the BPT hardware setup and safety measures taken will be described in detail.

4.1 BPT Transmit Setup

The BPT motion tracking method, as described in chapter 3, consists of two microwave tones transmitted throughout the MR exam [1][2][5]. For all of the experiments described in this work, we used two USRP Ettus Research B200 Software-Defined Radios (SDRs) synchronized to the MR system's 10 MHz clock to generate the two microwave tones. The two signals were combined, amplified, and band-stop filtered prior to transmission (Figure 4.1). The amplifier was necessary in order to drive the preamps to the nonlinear regime for intermodulation to occur, while the filter ensured that no intermodulation from the transmit amplifier was present in the transmitted signal. Lastly, floating cable traps were placed on the coaxial cable to attenuate common-mode currents induced on the cable's shield due to the transmit RF [1][17]. The antenna choice and placement varied throughout our experiments and will be discussed later in this section. The full BPT hardware set up is shown in Figure 4.1 and Figure 4.2.

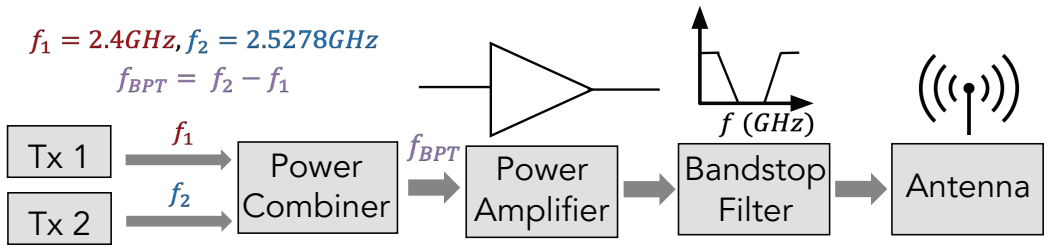

Figure 4.1: A diagram of the hardware setup used to transmit the BPT. Two microwave tones were generated with two USRP B200 SDRs. They were then combined, amplified, and band-stop filtered prior to transmission. The BPT was transmitted with an antenna placed inside or near the bore [5].

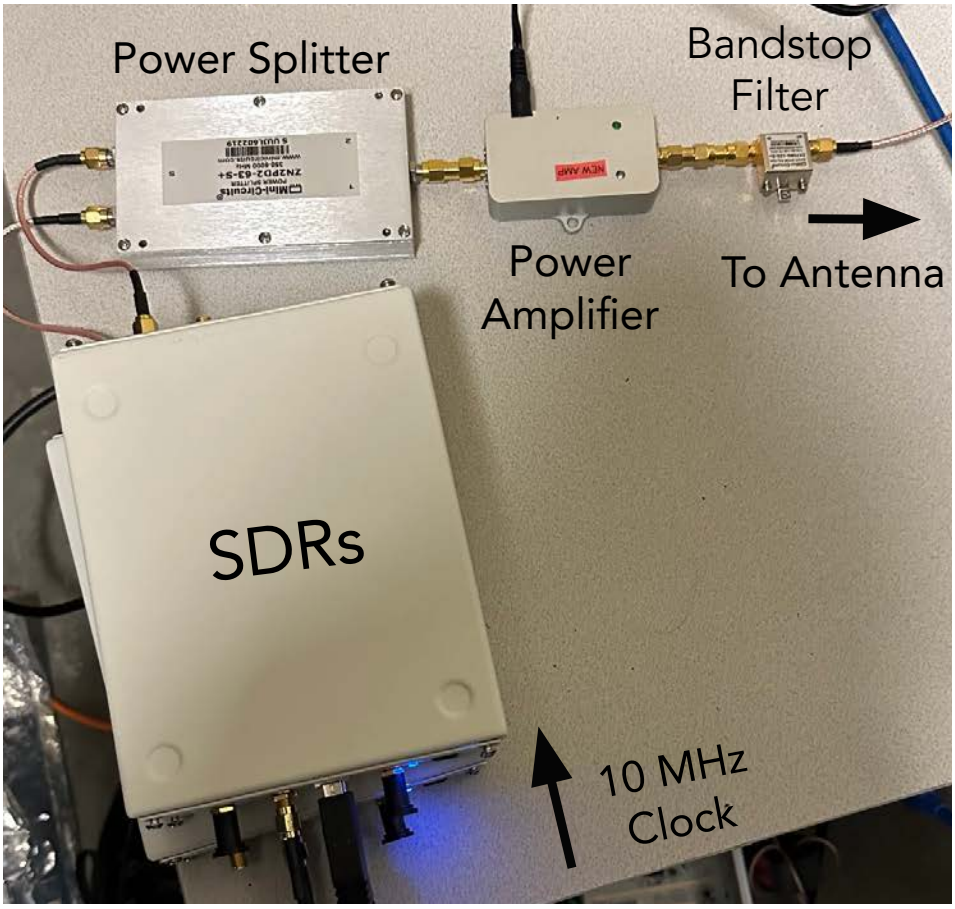

Figure 4.2: A photograph of the physical BPT hardware setup used to transmit the BPT. Each element of the transmit chain is labeled.

4.2 Cable Trap Fabrication

The MRI scanner produces a strong RF transmit field, which can induce common mode currents on any cable placed inside the scanner. If these cables come into contact with the subject, they can cause dangerous RF burns. Cable traps must be placed on any coaxial cable in an MR environment that may have contact with the subject in order to prevent these common mode currents from traveling along the coaxial cable [17]. A floating cable trap design, inspired by Fischer et al [17] [18], was constructed and placed on the coaxial cable leading to the BPT transmit antenna. The traps were 3D printed and then assembled as shown in Figure 4.3 and Figure 4.4 respectively. The assembly process included tuning the cable traps to provide resonant blocking at the B_1 transmit (Larmor) frequency and shielding the traps from heating due to the transmit RF. The traps were tuned by soldering capacitors to the middle slots. The shields were created by applying copper tape to the outer surface of the 3d-printed shield former. A Keysight Fieldfox Vector

Network Analyzer was used to tune the traps and ensure that 15 dB or higher blocking was achieved at the Larmor frequency.

Figure 4.3: The cable traps were created by 3D printing formers on which copper tape was applied. The left image shows the modeled formers in the 3D printer software, the middle image shows them after 3D printing, and the right image shows them after UV curing [2].

Figure 4.4: The cable traps were composed of a main body and outer shield to prevent them from heating due to the transmit RF field. The body and shield of a sample cable trap are shown in the middle and right images [2].

4.3 Cable Trap Safety Testing

The ability of the traps to ensure subject safety throughout the MR exam is crucial; therefore, rigorous safety tests are executed to examine whether the traps successfully prevent common mode currents from traveling along the coaxial shield and to verify that the cable traps maintain a safe temperature. In order to test the trap's ability to block common mode currents, a $\mathbf{B_1}$ map was attained with the traps secured

to the coaxial cable. $\mathbf{B_1}$ maps provide a measurement of the homogeneity of the $\mathbf{B_1}$ transmit field. In the event that the traps do not successfully block the current resulting from the transmit RF, then one will see distortions in the $\mathbf{B_1}$ map along where the coaxial cable was placed. For the $\mathbf{B_1}$ mapping experiment, a $\mathbf{B_1}$ map of a nonloading MR phantom was attained first with the cable (and traps) and then without. Figure 4.5 shows the placement of the phantom and cable for the trial with the cable and traps. The phase of the $\mathbf{B_1}$ maps for the slices indicated by the green bars on the phantom for both trials are also shown in Figure 4.5.

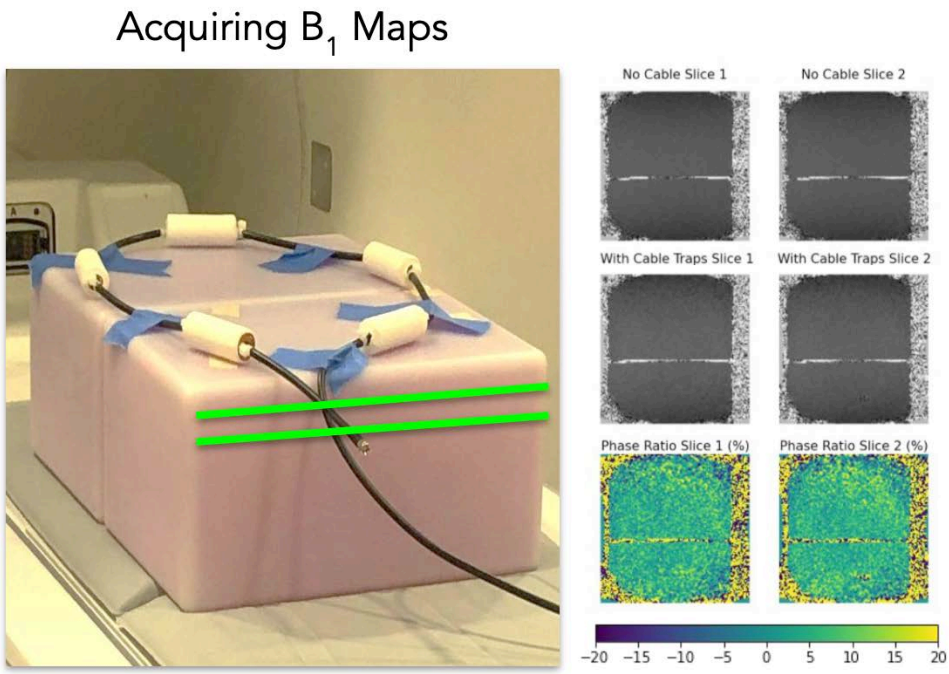

Figure 4.5: We acquired a $\mathbf{B_1}$ map with the traps secured to the coaxial cable to ensure that the traps did not distort the transmit field [2]. The left image shows the setup, which consists of a cable with traps on a nonloading MR phantom. The right images are the resulting $\mathbf{B_1}$ phase maps for the slice locations indicated on the left in green with and without the cable present. The bottom right result shows that the phase ratios for the slices with and without the cable present are within 30%, as desired.

Equation 2: B_1 Map Phase Ratio

$$\text{Phase Ratio} = \frac{\text{phase without coaxial cable}}{\text{phase with coaxial cable + cable traps}}$$

Lastly, Figure 4.5 shows the phase ratio of the $\mathbf{B_1}$ maps for each slice. The phase ratio shows how much the cable and traps distort the $\mathbf{B_1}$ field relative to when only the phantom is placed in the scanner. A $\mathbf{B_1}$ map phase ratio that shows a less than 30% deviation from the $\mathbf{B_1}$ map without the coaxial cable and traps indicates that the traps' ability to prevent this distortion (by blocking the common mode current) is within the typical $\mathbf{B_1}$ variation observed at 3T. We find this to be the case for the phase ratio maps we attained (see Figure 4.5, bottom right).

In addition to measuring the homogeneity of the $\mathbf{B_1}$ field, a heat test was also performed in order to determine whether the cable traps were at risk of overheating throughout an MR exam. The heat test consists of a gradient echo sequence (TE = 7 ms, TR = 18 ms, FA= 90°) that applies frequent RF pulses and is repeated over 16 minutes. We placed the cable and traps in the scanner in the three most common positions and ran the heat test. We measured the rise in temperature multiple times throughout the scan using a FLIR Thermal Camera. As shown in Figure 4.6, the temperature of the two traps closest to the antenna, which were the most prone to heating, stayed under $40°C$, which is required by the Institutional Review Board (IRB) for volunteer scans.

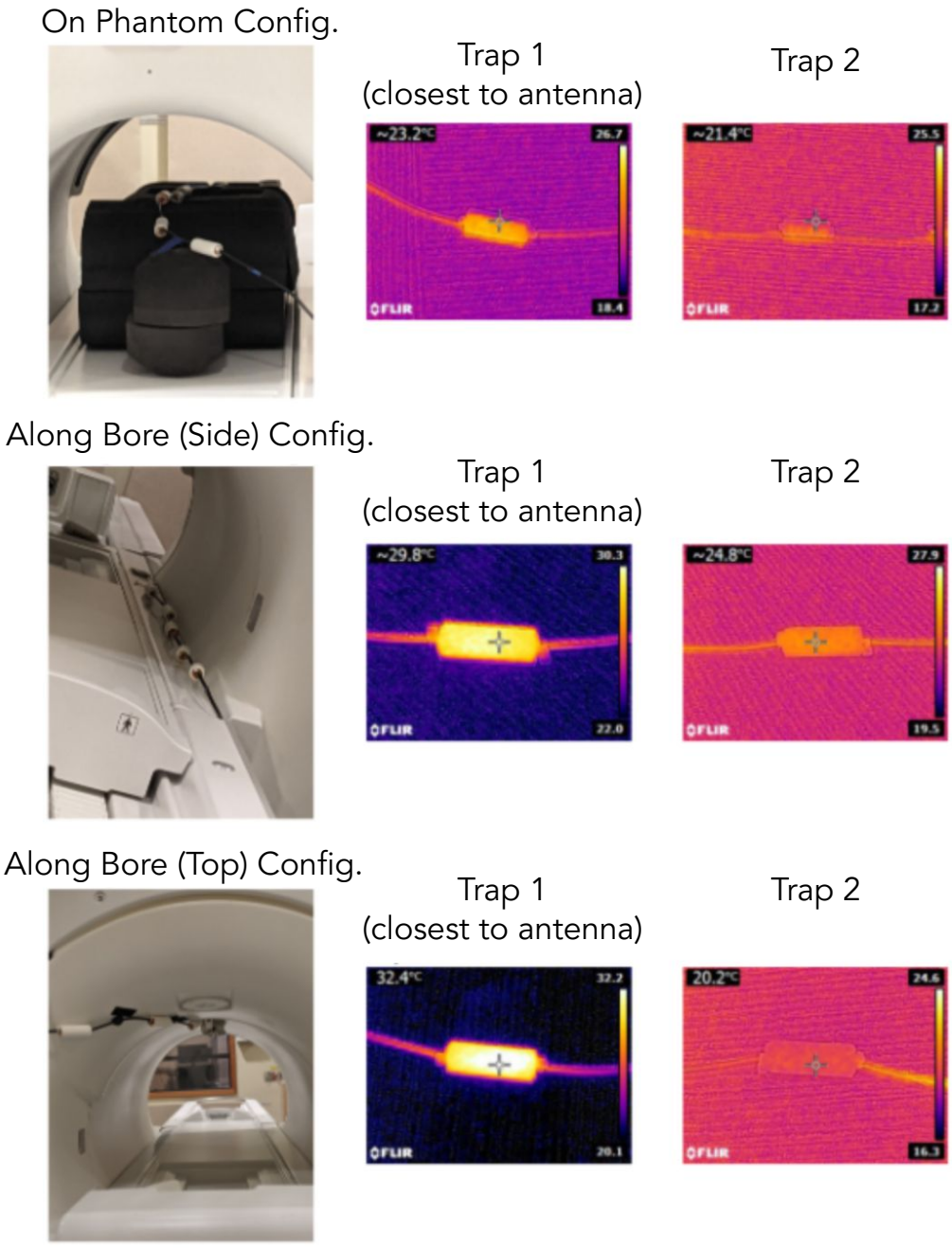

Figure 4.6: We performed a test to measure the heating of the traps over the course of 16 minutes. We placed the cable and traps in the scanner in the three most common positions, ran the heat test, and measured the rise in temperature multiple times throughout the scan using a FLIR Thermal Camera [2]. The configurations and their corresponding temperatures are shown on the left and right, respectively.

4.4 Gradient-Induced Artifacts

The BPT appears to be susceptible to gradient-induced artifacts that we have not seen in the PT signal [1][5][8][9]. We hypothesize that the BPT is sensitive to small perturbations of the antenna. These perturbations appear more prominently when the antenna is placed inside the bore due to both the gradient-induced eddy currents on the antenna, which cause the antenna to vibrate as a result of the Lorentz forces from the B_0 field, and due to the physical vibrations of the MR scanner. The source of the artifact is still under investigation and further experiments are needed before we can confidently say that these artifacts are caused by antenna vibrations induced by the gradients.

We chose to place the BPT antenna outside the bore for our real-time sequence in order to reduce the artifact in the BPT signal, allowing us to utilize less time-expensive processing methods. Figure 4.7 shows the BPT antenna setup used for the experiments discussed in chapter 7.

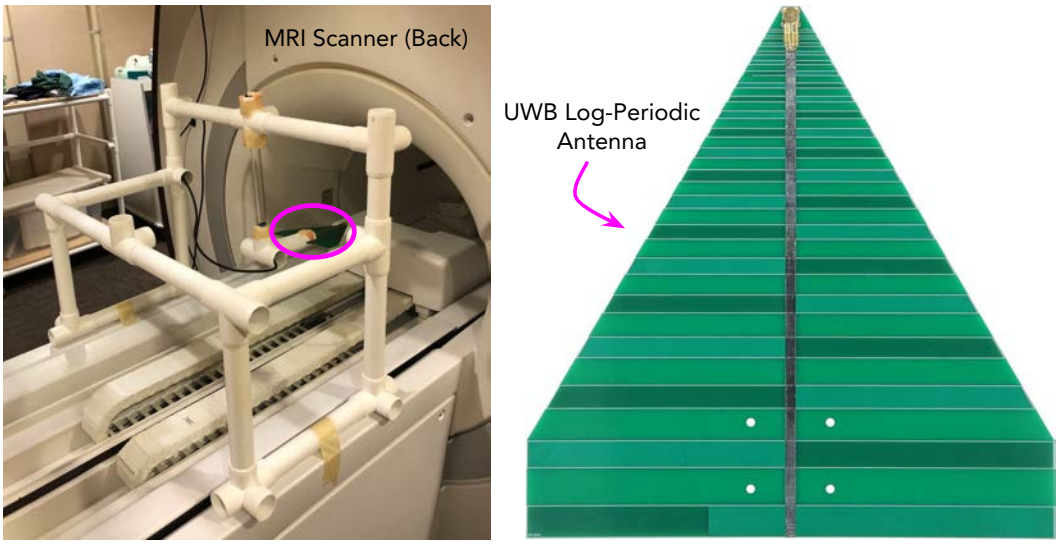

Figure 4.7: BPT Antenna Apparatus

Chapter 5

RETROSPECTIVE RESPIRATORY & CARDIAC MOTION CORRECTION USING THE BPT

Retrospective motion correction using a variety of motion tracking methods continues to be a very common and effective way for resolving cardiac and respiratory corrupted images. Researchers have made tremendous strides to utilize the insights provided by ECG, PPG, and respiratory bellows to further improve and develop new retrospective techniques. Although these methods have been shown to be quite robust, they are often only as good as the motion estimates they receive. In order to fully represent the motion that occurs throughout an MR exam, one must utilize a suite of sensors to capture both rigid and non-rigid motion. The sensors tend to leave the subject feeling uncomfortable. Additionally, the subject's motion could result in the sensors being tugged or misplaced, leading to inaccurate motion estimates. There have also been a number of cases of thermal injuries caused by ECG electrodes and PPG sensors [19]. The high sensitivity of the BPT for a wide range of motion along with the improvement in subject safety and comfort throughout the scan continues to make the BPT a very promising substitute for all of these motion tracking methods. In this section, we describe the methods used to compare the BPT to other motion sensors for retrospective cardiac and respiratory motion correction. This work was presented as a poster in the ISMRM 2022 Annual Meeting [1].

5.1 Retrospective Motion Correction Methods

A very simple motion correction method was implemented in order to validate the BPT's ability to provide cardiac and respiratory motion estimates comparable to standard cardiac and respiratory sensors (ECG and bellows). By demonstrating this notion, one can hypothesize that BPT motion estimates can replace the motion estimates provided by a suite of sensors (e.g. ECG, PPG, navigators, etc.) that many of the novel, machine learning-based cardiac and respiratory motion compensation techniques regularly rely on.

The method we used is known as "binning". It assumes that the underlying motion is periodic. Thus, data is sorted into motion states or different parts of the motion cycle based on amplitude or time. Each motion state is referred to as a bin. The data in each bin is then averaged to yield artifact-free images.

The BPT retrospective motion correction pipeline consists of extracting the BPT from the MR data as shown in chapter 3, selecting and processing the BPT waveform, binning the MR data into respiratory or cardiac motion states using the BPT motion estimates, and finally, averaging over the data in each bin to produce cardiac and respiratory resolved images [1]. This process yields a series of motion-corrected images, each corresponding to a particular motion state. Once the BPT was extracted from each coil, the BPT waveform from the coil with the most energy in the respiratory frequencies was selected for the abdominal scans and low-pass filtered with a cutoff of 0.5Hz [1]. For the cardiac scans, the BPT waveform from the coil with the most energy in the cardiac frequencies was selected and bandpass filtered between 5 and 15Hz [1].

A summary of the retrospective motion binning methods used for the cardiac and abdominal scans in this work is shown in Figure 5.1. We utilized the reconstruction method described in Figure 5.1 to provide motion-resolved images for each of the motion sensing methods examined in this work (BPT, PT, ECG, and respiratory bellows). For the abdominal scans, we binned the raw kspace data into motion states based on the amplitude of the motion signal for each TR of data. For the cardiac scans, we binned the raw kspace data into motion states based on time for each TR of data. Lastly, the data in each motion bin was averaged and then coil-combined using the root sum of squares (Algorithm 1) to obtain the motion-resolved images.

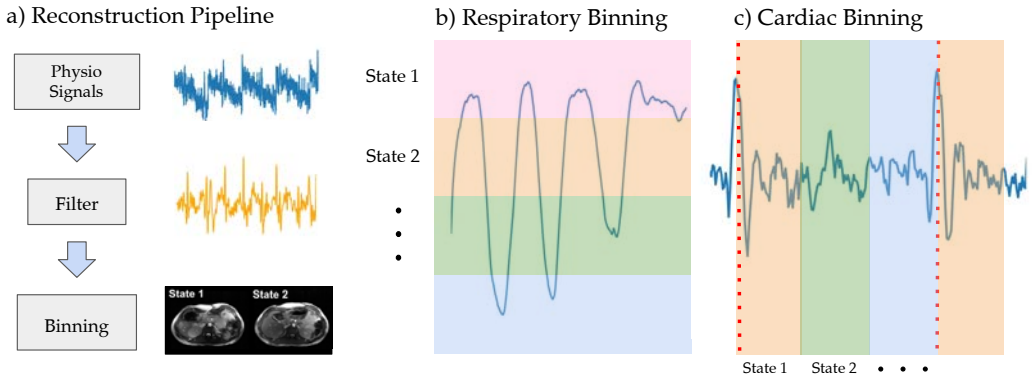

Figure 5.1: a) A summary of the reconstruction pipeline used for binning respiratory and cardiac data. The signals were filtered, then used to bin data into different motion states. b) We binned the data in to respiratory motion states based on amplitude. b) We binned the data into cardiac motion states based on time [1].

Algorithm 1 Root Sum of Squares [2]

Ensure: C = number of coils
Ensure: data = MR Data ▷ data is an array of shape (M, N, C)
$rss \leftarrow zeros[M][N]$; ▷ array of all zeros with shape (M,N)
$i \leftarrow 0$;
$j \leftarrow 0$;
$k \leftarrow 0$;
for $i < M$ **do**
  $j \leftarrow 0$;
  for $j < N$ **do**
    $k \leftarrow 0$;
    for $k < C$ **do**
      $rss[i][j] \leftarrow rss[i][j] + data[i][j][k] \times data[i][j][k]$;
      $k \leftarrow k + 1$;
    end for
    $rss[i][j] \leftarrow \sqrt{rss[i][j]}$
    $j \leftarrow j + 1$;
  end for
  $i \leftarrow i + 1$;
end for
$data \leftarrow rss$

5.2 Abdominal Imaging

A free-breathing, balanced SSFP sequence (TR=5.8 ms, FA=35, resolution=1.4mm, BW=250kHz) was acquired on a healthy volunteer with both the BPT (2.4 GHz, 2.5278 GHz) and PT (127.8 MHz). A panel antenna placed on a 32-channel anterior and posterior array coil was used to transmit both the BPT and PT signals. We also had the volunteer wear respiratory bellows during the scan as well. The motion estimates provided by the BPT, PT, and respiratory bellows data are shown in Figure 5.2. The signals provided by both the BPT and PT (raw and processed) are comparable to the respiratory bellow's motion estimate.

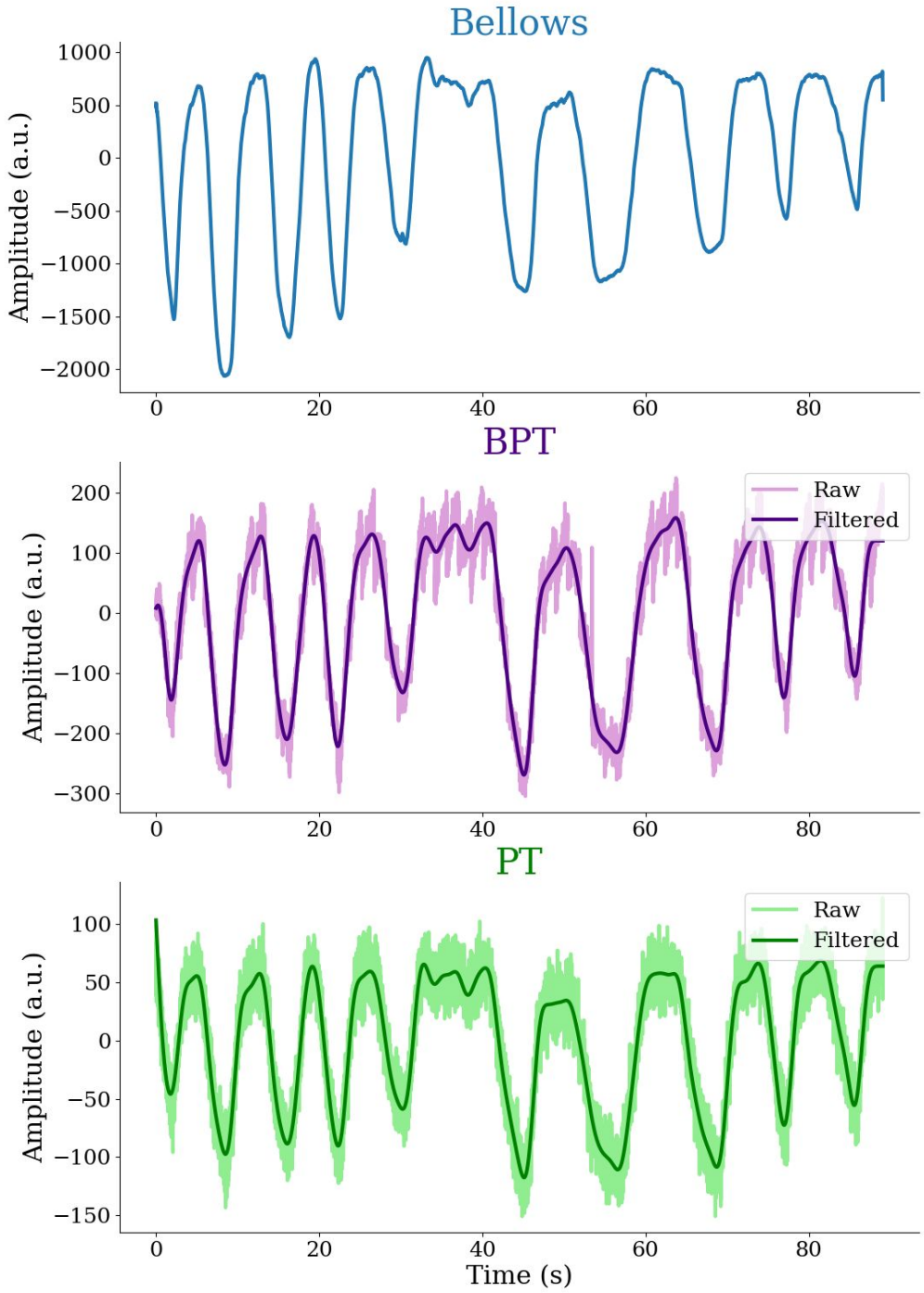

Figure 5.2: Respiratory Motion estimates for respiratory bellows, BPT, and PT [1]. The top plot shows the bellows signal over time. The bottom two plots show the unfiltered BPT and PT, respectively, with filtered signals overlaid. All signals are comparable in quality.

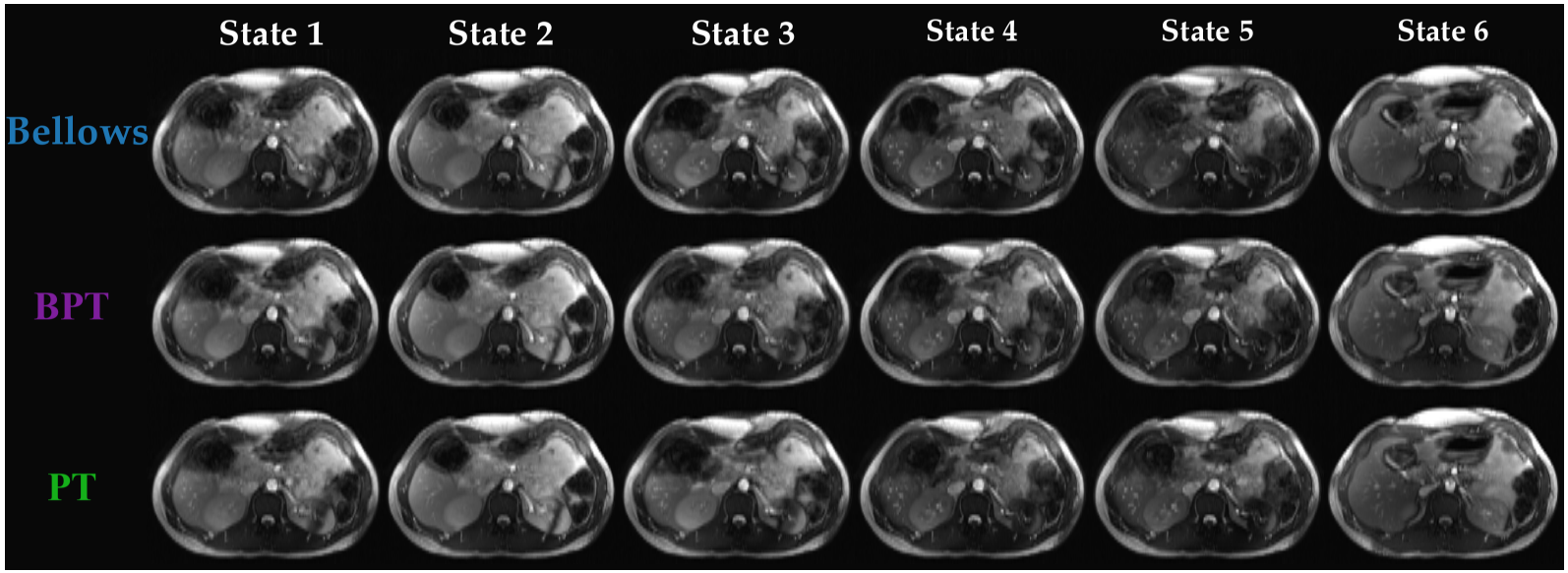

Figure 5.3: The reconstructed images after binning are shown for bellows, BPT, and PT [1]. Six motion states were chosen. All images appear to have comparable image quality.

The respiratory-resolved motion states using motion estimates provided by BPT, PT, and respiratory bellows are shown Figure 5.3. The motion signals were each used to bin the raw MR data into six motion states. The BPT and PT corrected motion states are comparable to the motion states corrected by the respiratory bellows. The BPT and PT, unlike the respiratory bellows, are able to sense other types of motion (cardiac, bulk motion, etc.), thus making RF-based motion tracking a more desirable option.

5.3 Cardiac Imaging

We acquired two breath-held scans using a balanced SSFP acquisition (FIESTA, TR=5.8 ms, FA=35, resolution=1.4mm, BW=250kHz). The first scan was acquired without gradients or RF excitation to avoid gradient-induced artifacts in the BPT signal. We also acquired ECG data simultaneously in order to compare BPT to ECG. Similar to the ECG, the BPT magnitude shows sharp, consistent peaks (Figure 5.4). In this figure, the peaks of the BPT were manually aligned to overlap with the ECG; however, in reality, there is some delay [3]. The BPT, unlike the ECG, does not actually measure the electrical signal of the heart; rather, the BPT seems to measure the heart's mechanical motion [1][3]. The BPT is hypothesized to provide a ballistocardiogram (BCG) signal, which shows surface vibrations of the body due to the ballistic forces of blood pumping through it [3]. Researchers have shown that BCG data provides additional information regarding the cardiac cycle and therefore may serve as an excellent substitute for ECG [20].

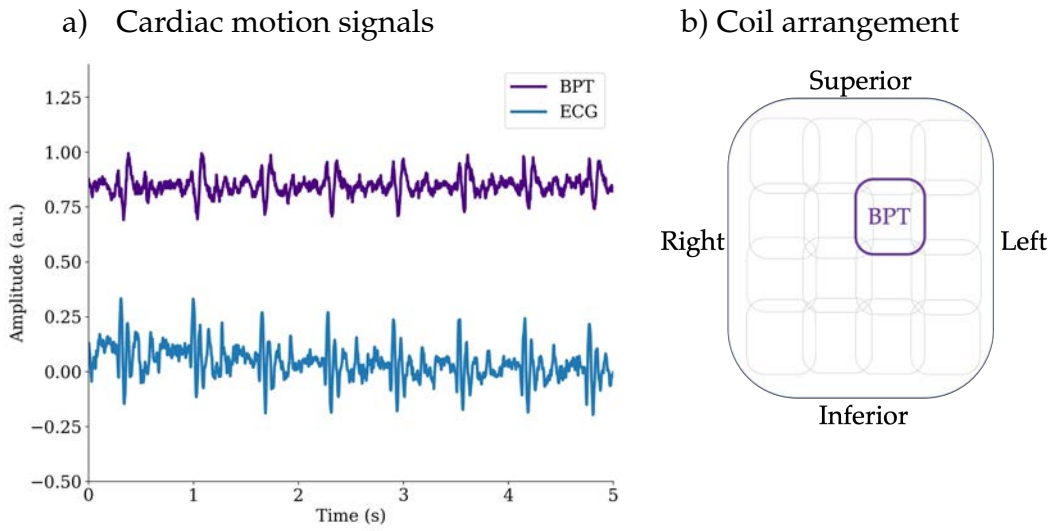

Figure 5.4: The BPT was acquired simultaneously to the ECG on a volunteer during a breath-held scan with imaging gradients off [1]. a) The unfiltered and mean-subtracted magnitude of the BPT is shown compared to ECG. The peaks of the BPT were manually aligned to overlap with the ECG; however, in reality, there is some delay. The BPT shows sharp peaks in the signal that could reveal information about the cardiac cycle. b) The physical location of the coil from which the BPT signal was chosen.

The second breathheld scan was also acquired with both the BPT and ECG with gradients and RF excitation on. The MR data collected was binned into five motion states based on the bandpass filtered BPT signal using the cardiac binning method described in Figure 5.1. The gradient-induced artifact is clearly visible in the raw BPT signal shown in Figure 5.5. The cardiac motion has a frequency that is close to the frequency of the gradient-induced artifact; therefore, it is more difficult to separate the motion from the artifact by simple filtering compared to the respiratory motion case. The bandpass filtered BPT signal shows more of the cardiac motion characteristics that the ECG provides; however, the artifact is still prominent and seems to reduce the accuracy of the binning. In Figure 5.6, the cardiac-resolved motion states attained using ECG and BPT are shown. The bandpass filtered BPT provides images comparable to the images attained when using the ECG for cardiac binning. The green arrows identify a few areas where the motion artifact is more prominent for the BPT-corrected images in comparison to the ECG-corrected images; however with additional processing techniques, these images can be improved.

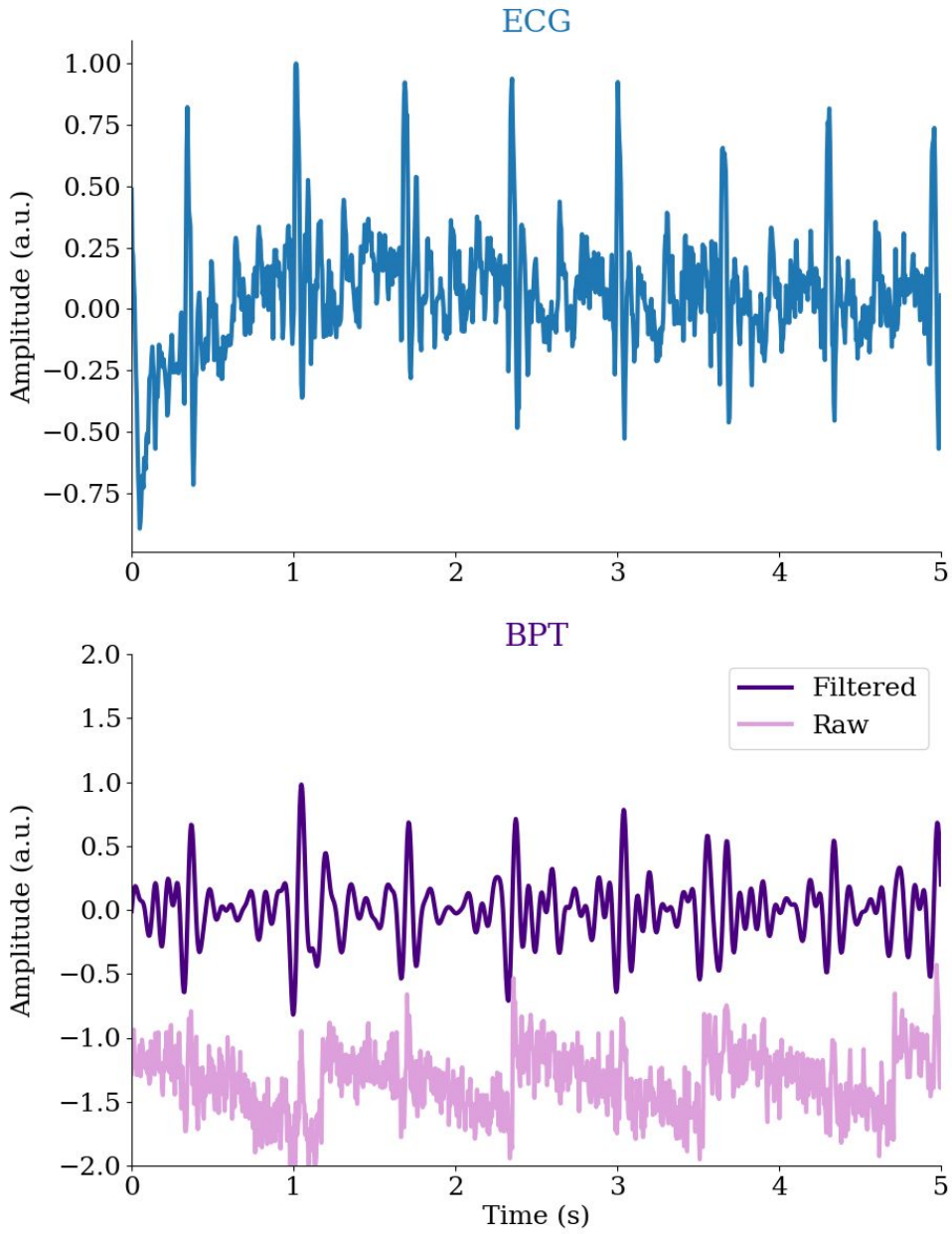

Figure 5.5: BPT and ECG Cardiac Motion Estimates are shown above. We can see that the gradient-induced artifact is very prominent in the raw data (light purple). The artifact is greatly reduced after applying a bandpass filter between 5Hz and 15Hz to the BPT signal; however, the artifact is still present [1].

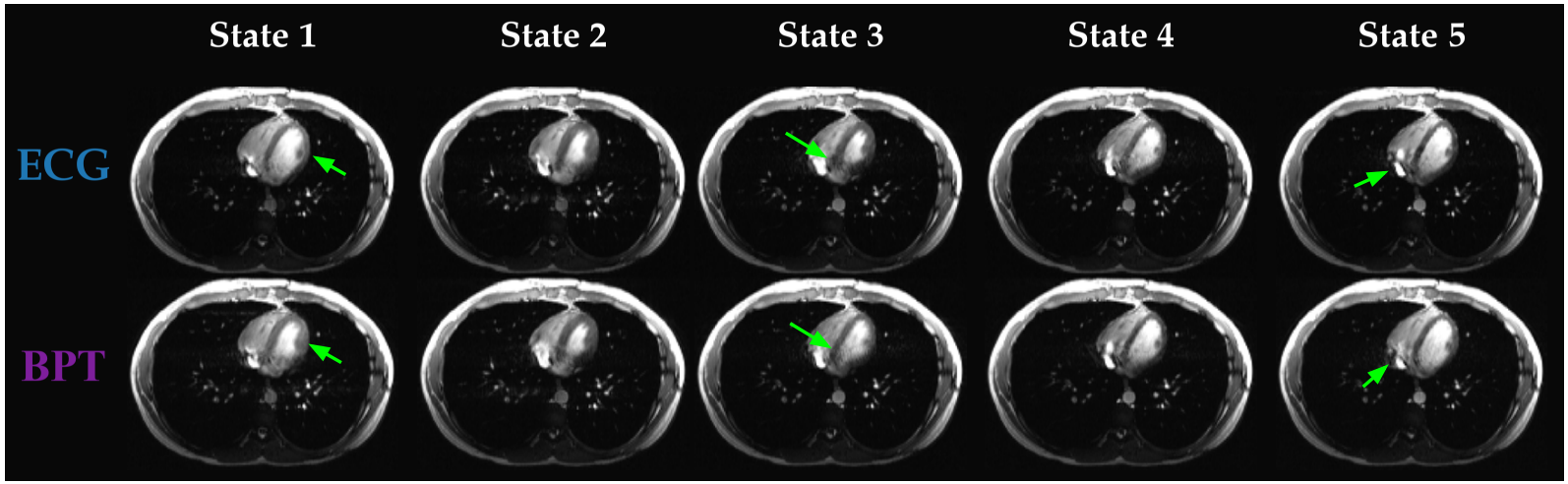

Figure 5.6: The cardiac-resolved motion states using the motion estimates provided by the bandpass filtered BPT signal is shown. The green arrows identify a few areas where the motion artifact is more prominent for the BPT-corrected images in comparison to the ECG-corrected images; however with additional processing techniques, these images can be improved [1].

We applied additional processing techniques to the BPT data to help remove the gradient-induced artifacts. The artifact was estimated using a linear fit and subtracted out of the BPT cardiac signal [1]. Figure 5.7 compares the original BPT to the BPT after different processing techniques were applied. The red signal is the BPT after the artifact estimate was removed from the BPT signal and after the bandpass filter was applied. We then used this BPT signal to bin the raw kspace data into five motion bins. Figure 5.8 shows the cardiac motion resolved images using the ECG and using the processed BPT signal. The green arrows point to the motion artifacts that were more severe for the BPT when only a bandpass filter was applied. We can now see that the motion artifacts have been reduced further and the cardiac-resolved images are almost identical to the corrected images provided by the ECG.

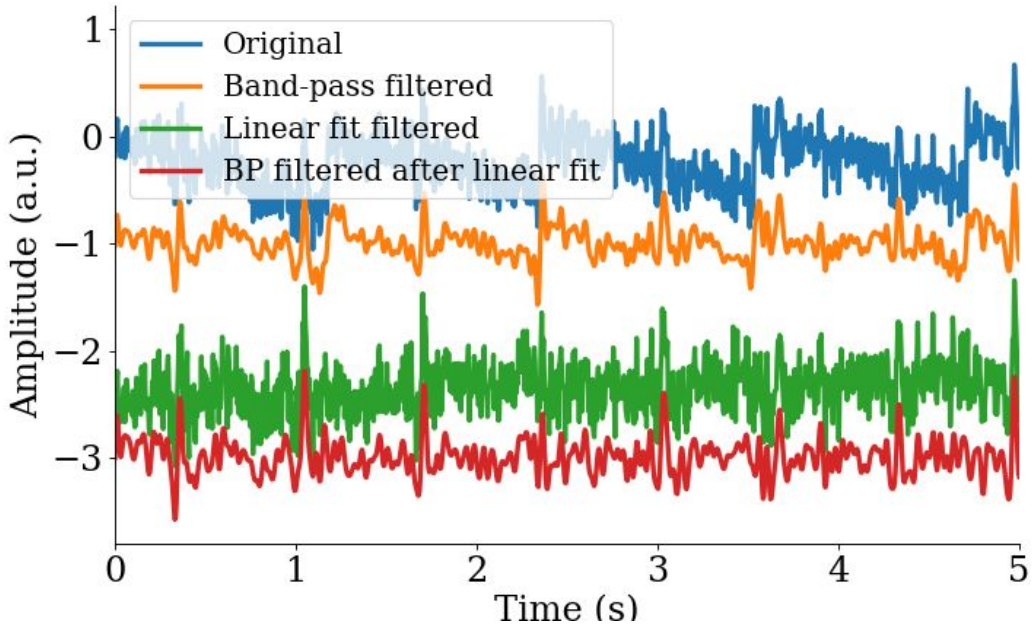

Figure 5.7: The original BPT cardiac signal (blue) along with the corrected signals attained by applying a variety of different artifact correction techniques to the original signal are shown above. The red waveform is the BPT signal after the gradient-induced artifact estimate was removed from the BPT signal and the resultant signal was then bandpass filtered between 5Hz and 15Hz. The signal was then used to attain the motion resolved images shown in Figure 5.8 [1].

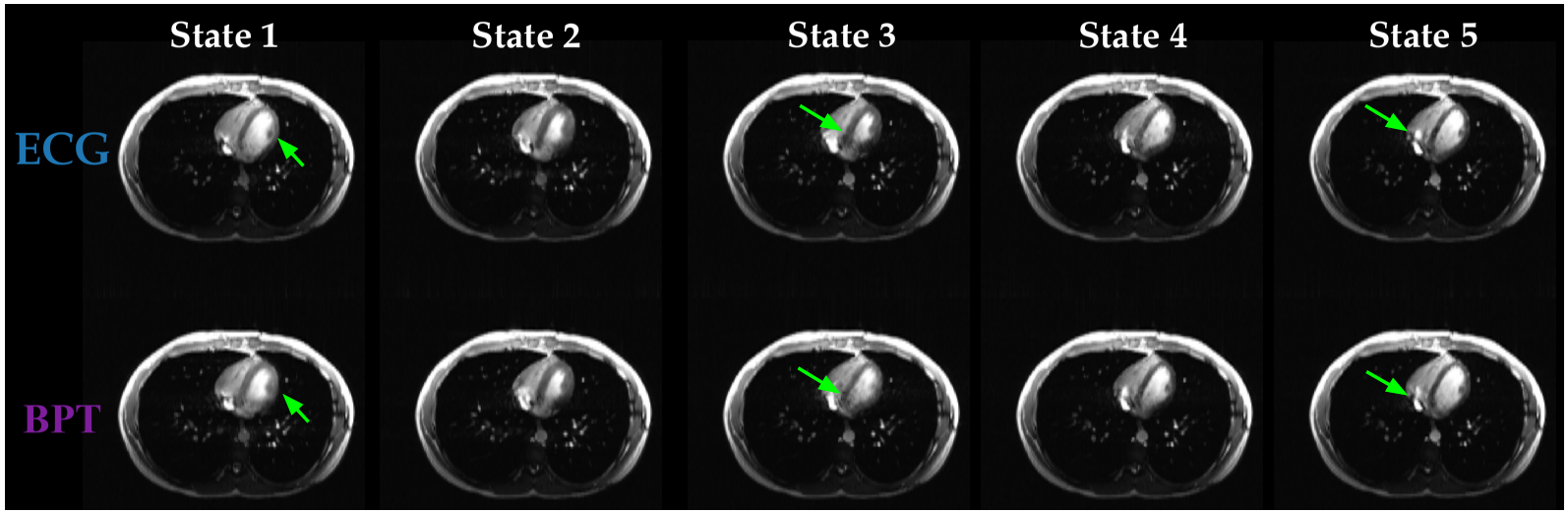

Figure 5.8: The cardiac-resolved motion states using the gradient-induced artifact corrected BPT signal is shown.The green arrows point to the motion artifacts that were more severe for the BPT when only a bandpass filter was applied. We can see that the motion artifacts have been further reduced and the results are comparable to the motion-resolved images attained using ECG motion estimates [1]

Chapter 6

REAL-TIME BPT PROCESSING USING RTHAWK

The BPT, as shown in previous sections, is able to sense a healthy volunteer's respiratory and cardiac motion with comparable quality to ECG, bellows, and PT. Replacing the sensors in the MRI suite with the BPT for both prospective and retrospective motion correction as well as for real time physiological signal tracking throughout the MR exam would improve subject comfort and safety and perhaps provide better quality sensor data. We, therefore, shifted our focus onto integrating the BPT into a suite of RTHawk Custom MR Research applications that can be run at a click of a button.

Vista.ai's RTHawk MR Research software provides researchers with the tools to make custom MR pulse sequences, implement real-time image reconstruction methods, and allow for endless flexibility when it comes to the user interface and visualization. RTHawk software is compatible with both GE and Siemens MR systems. A summary of the RTHawk architecture is provided in Figure 6.1.

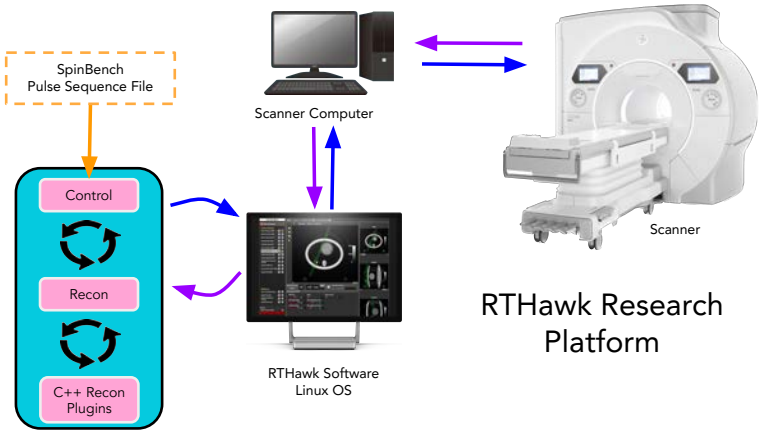

Figure 6.1: The RTHawk platform provides a path of communication between the scanner and the control, reconstruction ("recon"), and pulse sequence design files created by the user. On the control side of RTHawk, researchers can use convenient Javascript, real time sequencer commands to update scan parameters based on information acquired while the data is going through the user-defined reconstruction pipeline designed on the recon side of RTHawk. Additionally, RTHawk provides Spinbench pulse sequence software to aid in pulse sequence design and visualization.

RTHawk research software provides a plethora of scan control and image reconstruction C++ plugins that are easily accessible from the Javascript files associated with each RTHawk application. A reconstruction plugin that is capable of extracting and processing the BPT/PT in real time is, however, not available in the RTHawk library. We therefore created a BPT/PT extraction and processing plugin (bptFilter) that takes the 1D Inverse Fast Fourier Transform (FFT) of each readout line, extracts the BPT/PT data using Algorithm 2, normalizes the data, applies an optional low pass, bandpass, or high pass filter, and then does additional processing to combine data across coils. First, during a user-defined training period, Principle Component Analysis (PCA) is applied to the BPT magnitude data to extract a user-specified number of PCs. After the training period, new data is projected onto the learned components (Figure 6.2). Finally, the raw data for each coil as well as the data for each PCA component is sent to the UI and reconstruction pipeline.

Algorithm 2 BPT/PT Real Time Extraction

While Loading Application

bptFreq $\leftarrow$ 2527.750 – 2400 ▷ user defined in UI
centerFreq $\leftarrow$ getCenterFreq() ▷ scanner center frequency
BW $\leftarrow$ getBandwidth() ▷ sequence bandwidth
$N_r \leftarrow$ getNumReadouts() ▷ number of readouts
$N_c \leftarrow$ getNumCoils() ▷ number of coils
BWPP $\leftarrow \frac{BW}{N_r}$ ▷ bandwidth per pixel
j $\leftarrow \frac{\text{(bptFreq - centerFreq)}}{BWPP} + \frac{N_r}{2}$ ▷ bptIndex

Real Time Extraction

input $\leftarrow$ dataInStream ▷ one TR of data with size $N_r \times N_c$
output $\leftarrow$ dataOutStream ▷ 1 sample = array(N_c)
$i \leftarrow 0$
▷ Root Sum of Squares over 3 pixels for each coil
while $i < N_c$ **do**
    $\text{output}[i] \leftarrow \sqrt{\text{input}[j-1][i]^2 + \text{input}[j][i]^2 + \text{input}[j+1][i]^2}$
end while

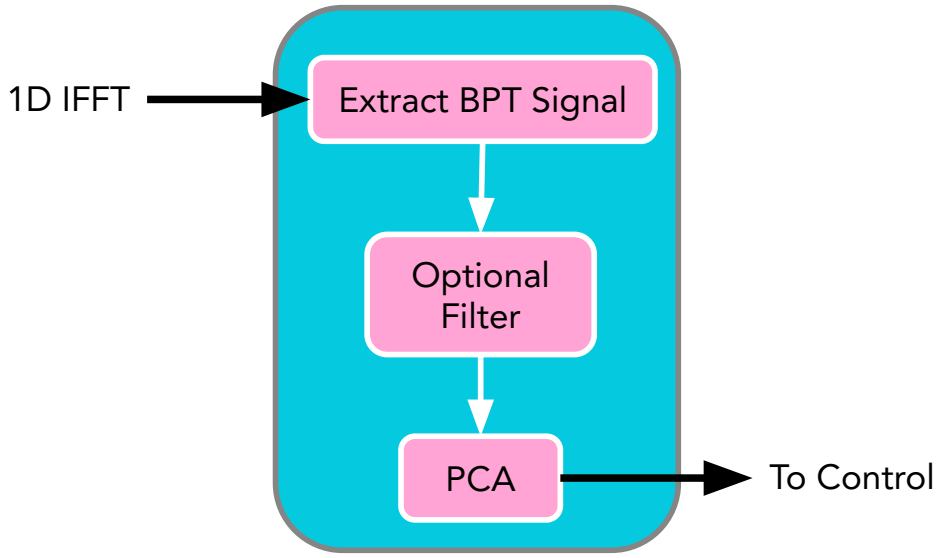

Figure 6.2: The RTHawk bptFilter Pipeline is first sent the MR data in real time (one TR at a time). The plugin extracts the BPT signal from each coil's MR data (see Algorithm 2) and applies an optional lowpass, highpass, or bandpass filter with the cutoffs specified by the user. The BPT data is projected onto the BPT's PCA components that were learned during the training period at the start of the scan in order to coil-combine the BPT data into a user-defined number of signals. The coil-combined BPT signal(s) along with the BPT signal from each coil are then sent to the control side of the RTHawk Platform in order to display the BPT waveforms on the UI.

The bptFilter plugin, once installed, can be integrated into any RTHawk application's reconstruction pipeline with minor changes to the application's UI using Qt5 Designer. Additionally, a custom BPT UI was created with two additional real time plot tabs to visualize the BPT/PT waveform from each coil on a single plot as well as to visualize the motion estimates after applying PCA (Figure 6.3). The optional filter can be set when initializing the bptFilter plugin in order to obtain motion estimates for certain types of periodic motion such as respiratory or cardiac motion. The UI also displays ECG and respiratory bellows signals in real time along with the MR images.

The bptFilter plugin is capable of triggering on the BPT/PT data and will send said information to the application's reconstruction and control. Access to this information allows for one to implement real time sequence updates based on whether a trigger has been received. An example of this type of triggering and real time scan control based on the BPT motion estimates is presented in chapter 7.

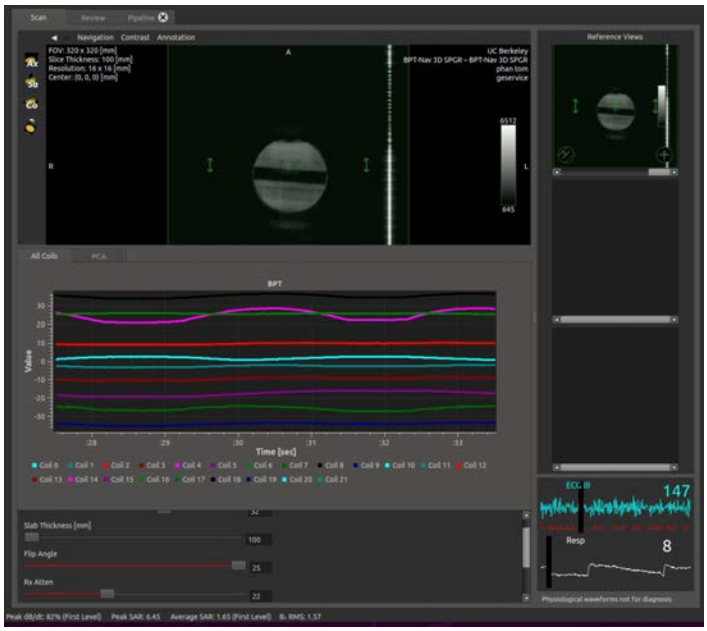

All Coils Display

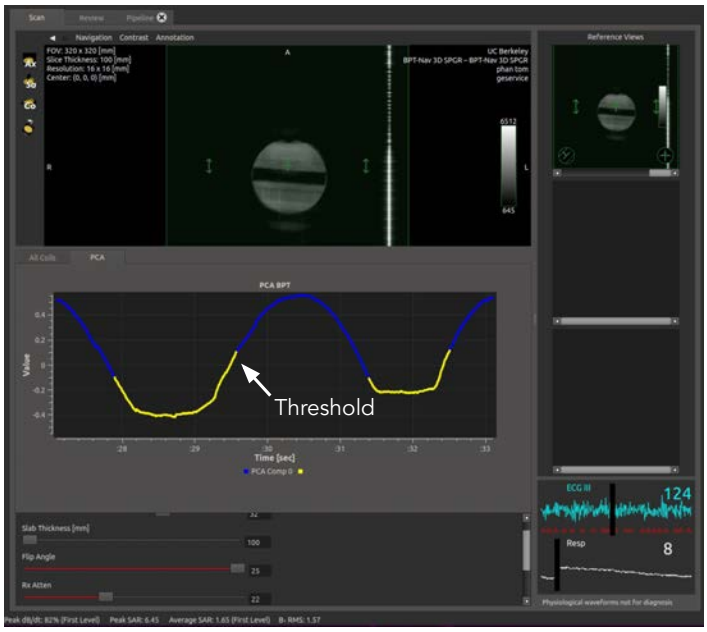

PCA with Thresholding Display

Figure 6.3: The Custom BPT User Interface for the RTHawk platform displays multiple real time physiological waveforms including the BPT, ECG, and respiratory bellows. Users can toggle between the All Coils Display which shows the BPT signal from each coil and the PCA with Thresholding Display which shows the BPT after applying PCA. The PCA with Thresholding Display also indicates when a threshold is met by changing the color of the waveform.

Chapter 7

PROSPECTIVE, FREE-BREATHING 3D SPGR MOTION CORRECTION

Three-dimensional (3D) MR scans, unlike 2D MR scans, can provide high-resolution volumetric and dynamic information; however, 3D acquisitions tend to be riddled with motion artifacts that are often very difficult to correct [21]. In particular, 3D abdominal scans are generally overwhelmed by respiratory motion artifacts [21]. Prospective, navigator-based correction methods are often applied to determine when to scan (e.g. during the least motion heavy segments of the respiratory cycle) as well as when to throw out a TR of kspace data altogether due to excessive motion corruption [21]. In this section, a prospective BPT-Navigated (BPT-Nav) 3D Spoiled Gradient Echo (SPGR) application will be introduced along with the details on how this application was implemented in RTHawk. We also validate the effectiveness of the BPT-Nav 3D SPGR sequence on phantom and volunteer scans.

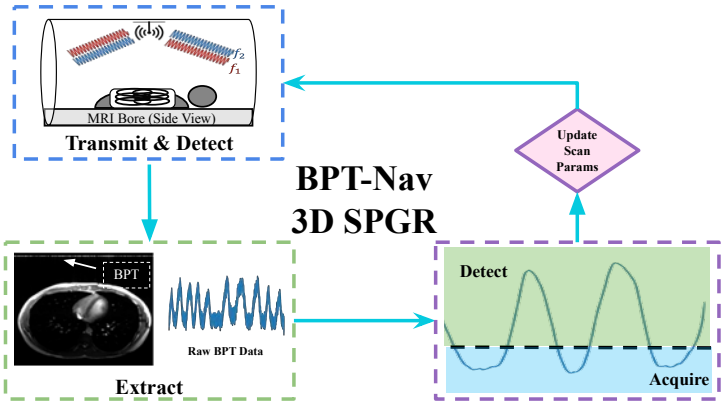

Figure 7.1: A summary of the BPT 3D SPGR Acquisition and Control Pipeline is provided. First, the data is acquired while the BPT is transmitted, as described in chapter 3. The k-space data is sent to the RTHawk Platform one sample at a time and processed to extract the raw BPT data ("Extract" block). We then low pass filter (0.5 Hz) each coil's BPT signal and coil-combine the data to obtain respiratory motion estimates. We use this data to determine whether we need to switch between Acquire and Detect modes based on a user-defined threshold. If the threshold is crossed, we update the scan parameters to switch to either Detect or Acquire.

7.1 BPT-Navigated 3D SPGR

In order to use the BPT motion estimates prospectively, one must continually acquire MR data to track the BPT motion signal. We therefore have two main acquisition modes: Detect and Acquire, as illustrated in Figure 7.1. The detect mode is used only for the purpose of tracking the BPT signal. In order to minimize gradient-induced artifacts, the detect mode does not increment the phase encode nor the z-encode and thus repeats the same gradient waveforms. We also placed the log-periodic antenna on the apparatus outside the bore, as shown in chapter 4, to prevent the antenna from vibrating, thus requiring less BPT processing after each TR. The data accumulated during the detect stage of the BPT-Nav 3D SPGR is plotted on the UI; however, the data is not used for the final image. We therefore updated the bptFilter plugin to discard TRs of data that were tagged with a "detect" label. One can easily tag the data with the "detect" label using RTHawk's real time sequencer commands on the Javascript side of the application. The full bptFilter plugin extract and process pipeline implemented for this application is shown in Figure 7.2.

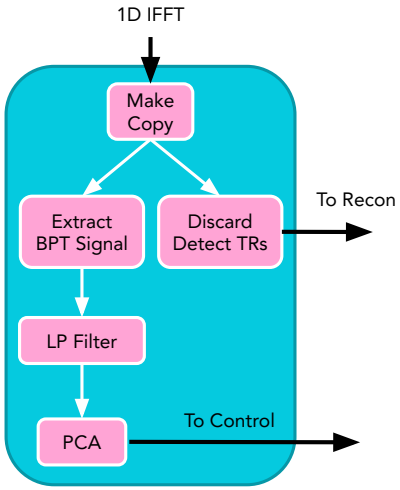

Figure 7.2: The RTHawk bptFilter Plugin Pipeline is shown above. The plugin first receives the 1D IFFT data (one readout at a time) and makes a copy of the data for BPT processing. The original data is discarded if the sequence is in Detect mode. If the sequence is in Acquire mode, the original data is sent to the recon pipeline. We extract each coil's BPT data from the copied data (See Algorithm 2). A lowpass filter with a cutoff of 0.5 Hz is then applied to each BPT signal. The PCA component used to coil-combine the BPT signals was learned on the first 10 seconds of data. After the training period, the BPT signal is projected onto the first principal component to attain the processed BPT signal. The signal is then analyzed to determine whether the threshold has been crossed, and this information is sent to the control side of the application in order to update the sequence accordingly.

The application decides to acquire data based on a threshold that is chosen by the user. Once the threshold is met, the application switches to the acquire mode, and the sequence progresses through the phase and z-encodes in a normal fashion until the threshold is met again. The threshold is set to indicate when the subject is towards the middle or end of their exhalation phase of the breathing cycle, which is when there is minimal respiratory motion. The RTHawk real-time control capabilities allows for one to send a signal (upon meeting the threshold) from the plugin to the control side of the application. Once the threshold was detected, real time sequencer updates from the control side of RTHawk initiated the switch between the two modes. The RTHawk-generated reconstruction pipeline is shown in Figure 7.3.

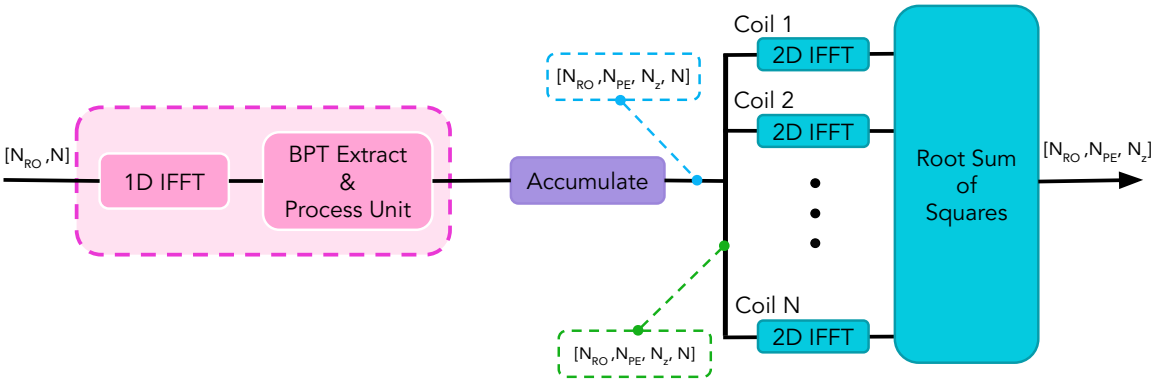

Figure 7.3: BPT-Nav 3D SPGR RTHawk Pipeline is shown. The pink pipeline elements are used for BPT extraction, and the blue pipeline elements make up the normal 3D recon pipeline. First, data accumulated during one readout is sent to the pipeline. A 1D IFFT in the readout direction is applied to the data, which is then sent to the BPT Extract and Processing Unit (i.e. the bptFilter Plugin) for BPT extraction and processing. During the Acquire mode, the same TR of data passed into the plugin is passed to the accumulation element of the pipeline (purple). Once all of the data for the 3D SPGR sequence is accumulated, the data is split along the coil dimension and a 2D IFFT is applied in the phase encode and z-encode dimensions. Finally, the root sum of squares (described in Algorithm 1) is applied to coil combine. **Note:** N_{RO} is the number of samples per readout, N_{PE} is the number of phase encodes, N_z is the number of z-encodes, and N is the number of coil elements.

7.2 BPT-Nav 3D SPGR Phantom Scans

The BPT-Nav 3D SPGR application was first validated by acquiring three scans on a phantom: one with no motion, one with motion and no correction, and one with motion that was prospectively corrected using the BPT as a navigator. The phantom was filled with doped water and contained small features made of plastic

such as the GE logo. To simulate motion, we used the GE "Rocker" tool, which moves the scanner bed periodically in the z-direction at a user-specified speed, displacement, and delay between movements. The rocker displaced the bed 15 mm at a peak rate of 15 mm/s. A 0.5 second delay was added each time the rocker switched directions (twice per cycle). The scan with no motion provides us with a ground truth. Figure 7.4 shows the results from the 3D SPGR phantom validation experiment. We can see that most of the motion artifact was removed when utilizing the BPT navigated sequence in comparison to the images without motion correction. We can improve upon these results by implementing more robust thresholding and outlier removal methods discussed in chapter 8.

7.3 Free-Breathing BPT-Nav 3D SPGR

To demonstrate the BPT-Nav 3D SPGR application in vivo, we acquired two prospectively corrected free-breathing scans on a healthy volunteer: one with BPT-Nav 3D SPGR implemented in RTHawk and one with GE's 3D LAVA ASPIR sequence using respiratory bellows. Figure 7.5 and Figure 7.6 show the results from the GE's 3D LAVA ASPIR and BPT-Nav 3D SPGR sequences, respectively. Since we did not choose the same scan parameters for each scan, we selected the images showing the same anatomy to include in both figures. We can see that the BPT-Nav 3D SPGR results are comparable to respiratory bellows-navigated LAVA scans; however, respiratory motion still considerably impacts the quality of both scans. There are quite a few ways that we can improve the BPT-Nav results including more robust thresholding and processing methods. We can also remove outlier motion and regularly update the PCA component throughout the scan to provide more accurate BPT motion estimates. We discuss these possible next steps in more detail in chapter 8.

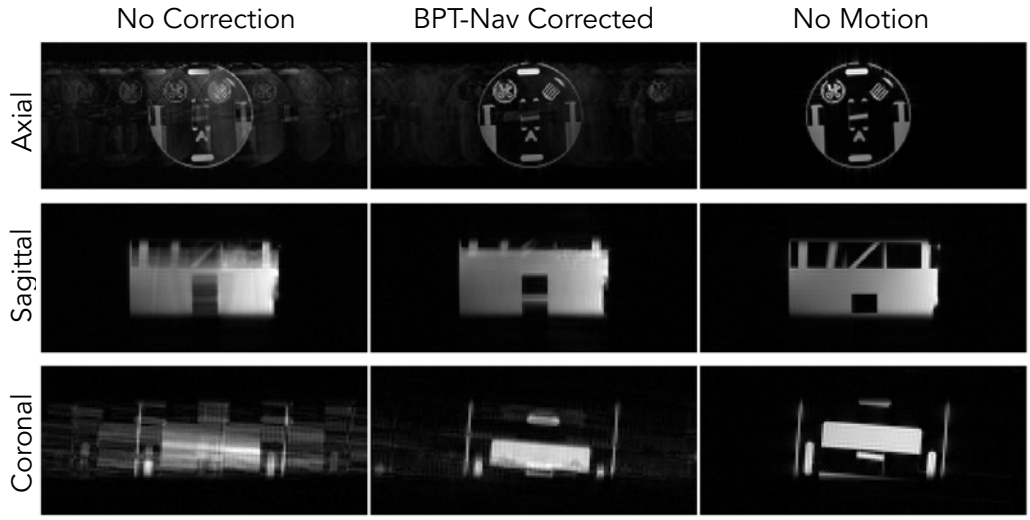

Figure 7.4: A single slice in the Axial, Sagittal, and Coronal planes for the no motion, motion without correction, and motion with BPT-Navigated prospective correction phantom scans are shown. *Scan Details:* TR: 8.784ms, FA: 25°, Resolution: 2.5mm x 2.5mm x 0.78mm, FOV: 50cm x 50cm x 5cm.

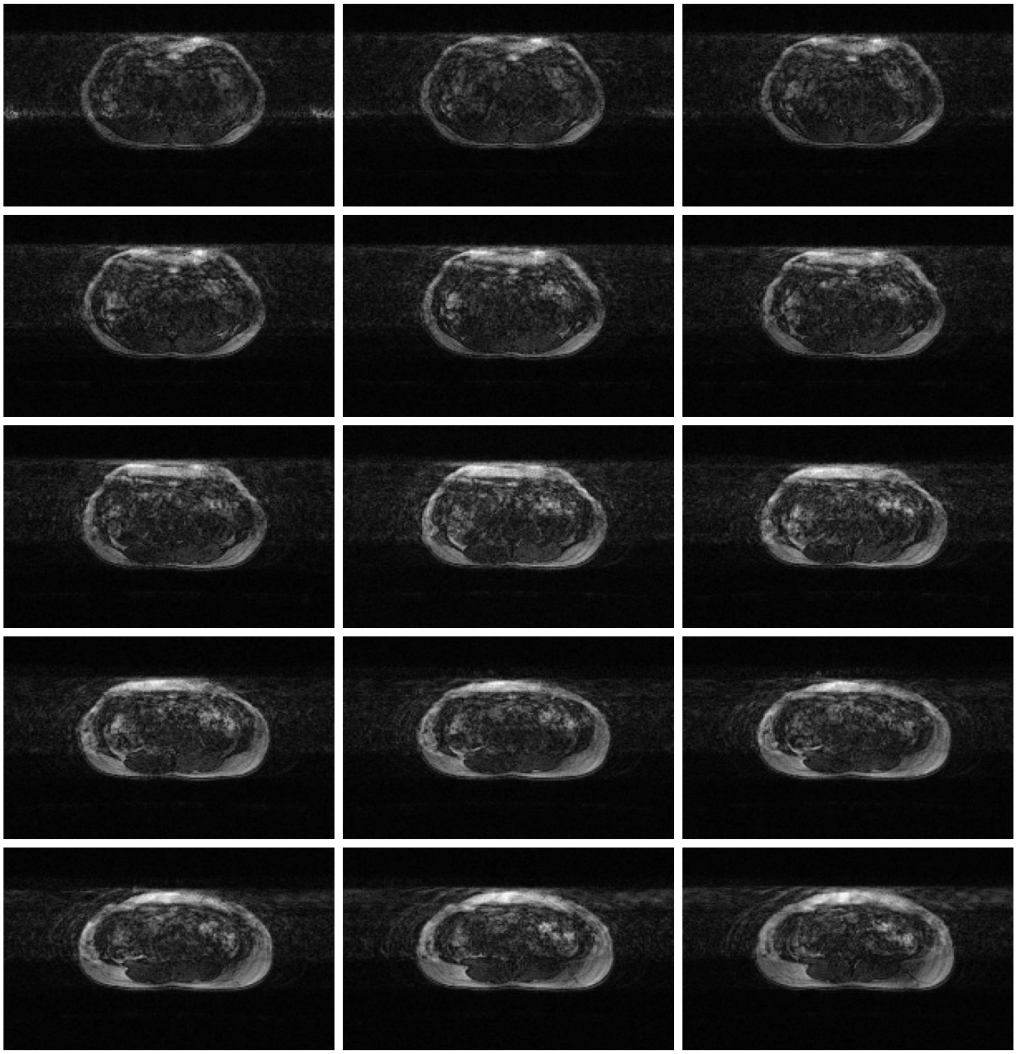

Bellows Navigated (LAVA)

Figure 7.5: The volunteer scan results for the respiratory bellows-navigated LAVA sequence are shown. *Scan Details:* Axial, TR: 6.8ms, FA: 25°, Resolution: 2.5mm x 2.5mm x 5mm, FOV: 50cm x 50cm x 32cm.

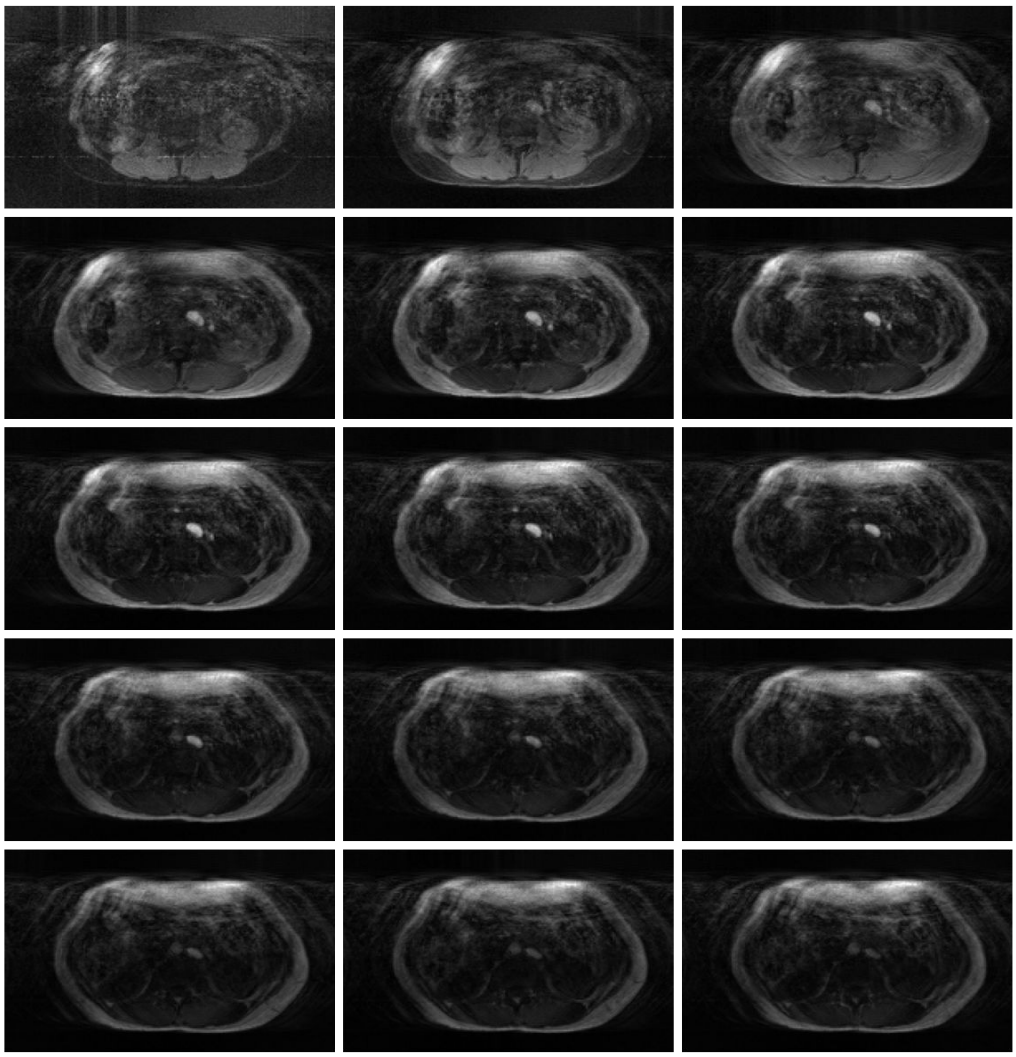

Figure 7.6: The volunteer scan results for the BPT-Nav 3D SPGR Application are shown. *Scan Details:* Axial, TR: 8.784ms, FA: 25°, Resolution: 2.5mm x 2.5mm x 1.56mm, FOV: 50cm x 50cm x 10cm.

Chapter 8

CONCLUSION & FUTURE WORK

The BPT is capable of providing respiratory and cardiac motion estimates comparable to conventional motion sensing methods (e.g. sequence navigators, respiratory bellows, ECG, and RF navigators). The BPT, unlike other motion sensing methods, does not require additional on-subject hardware and does not place constraints on the types of sequences or scan parameters that can be used. Additionally, the BPT provides high sensitivity and accuracy when it comes to tracking all types of motion including cardiac, respiratory, and bulk motion [1][3][5].

In this work, we first showed that BPT motion estimates can be used to retrospectively correct for both cardiac and respiratory motion. The respiratory motion-resolved images using the BPT were comparable to the images corrected using the respiratory bellows and the PT [1]. The BPT's high sensitivity to cardiac motion allowed for cardiac motion-resolved images comparable to the images corrected using the ECG cardiac motion estimates [1][3].

Lastly, this work took a first look at using the BPT to prospectively correct respiratory motion during a 3D SPGR sequence implemented in Vista.ai's RTHawk MR Research Platform. We showed that the motion-resolved images using the BPT navigator had significantly fewer motion artifacts compared to the images acquired without the navigator on a phantom. The BPT-Nav 3D SPGR application also provided similar in vivo results to the images acquired with GE's respiratory bellows-navigated LAVA sequence. Although these initial results are promising, in future work, we will need to equalize the imaging parameters (FOV, resolution, etc) between the BPT and LAVA acquisitions to ensure a fair comparison.

The prospective motion correction work we have done thus far has demonstrated the BPT's potential to be a substitute for respiratory bellows for motion tracking during free breathing abdominal scans. The initial results shown in this work can be further improved with more robust methods to determine a threshold for when to switch between the acquire and detect modes of the BPT-Nav 3D SPGR application as well as by updating the learned PCA components multiple times throughout the scan. In future work, we plan to move beyond using a simple threshold for sensing the exhale portion of the scan. We may utilize PCA to classify the BPT data, which will allow

the algorithm to identify when unexpected bulk motion (unrelated to the respiratory cycle) occurs. Once this type of motion is detected, the k-space data acquired can be discarded, and a signal can be sent to the scanner to re-acquire the data. We also plan to look into methods that will shorten the length of the scan (e.g. compressed sensing), resulting in a reduction in the amount of motion that can occur throughout the acquisition. Lastly, we plan to further investigate the BPT's ability to track cardiac motion by implementing a prospective cardiac cine application triggered on the BPT's cardiac motion estimates.

BIBLIOGRAPHY

[1] Kathryn Lamar-Bruno, Suma Anand, and Michael Lustig. "Retrospective Motion Correction in Magnetic Resonance Imaging using the Beat-Pilot Tone". In: *UC Berkeley Mathematics Honors Thesis* (2022).

[2] Kathryn Lamar-Bruno. *Retrospective Motion Correction in Magnetic Resonance Imaging using the Beat-Pilot Tone*. Tech. rep. University of California, Berkeley, 2022.

[3] Suma Anand and Michael Lustig. "Wireless In-Bore Ballistocardiography with 2.4GHz Beat Pilot Tone (BPT)". In: *ISMRM Meeting and Exhibition Abstract* (2023).

[4] Julian Maclaren et al. "Prospective motion correction in brain imaging: a review". In: *Magnetic resonance in medicine* 69.3 (2013), pp. 621–636.

[5] Suma Anand and Michael Lustig. "Beat Pilot Tone: Exploiting Preamplifier Intermodulation of UHF/SHF RF for Improved Motion Sensitivity over Pilot Tone Navigators". In: *ISMRM Meeting and Exhibition Abstract* (2021). URL: https://cds.ismrm.org/protected/21MPresentations/abstracts/0568.html.

[6] Dwight G. Nishimura. *Principles of Magnetic Resonance Imaging*. Lulu.com, 2010.

[7] Florian Thiel et al. "Combining magnetic resonance imaging and ultrawideband radar: a new concept for multimodal biomedical imaging." In: *The Review of scientific instruments* 80 1 (2009), p. 014302.

[8] Eddy Solomon et al. "Free-breathing radial imaging using a pilot-tone radiofrequency transmitter for detection of respiratory motion". In: *Magn Reson Med.* (2021). DOI: https://doi.org/10.1002/mrm.28616.

[9] Juliane Ludwig et al. "Pilot tone–based motion correction for prospective respiratory compensated cardiac cine MRI". In: *Magn Reson Med* (2021). DOI: https://doi.org/10.1002/mrm.28580.

[10] Aaron T Hess et al. "Diaphragm position can be accurately estimated from the scattering of a parallel transmit RF coil at 7 T". In: *Magnetic resonance in medicine* 79.4 (2018), pp. 2164–2169.

[11] D Buikman, T Helzel, and P Röschmann. "The rf coil as a sensitive motion detector for magnetic resonance imaging". In: *Magnetic resonance imaging* 6.3 (1988), pp. 281–289.

[12] Sven HF Jaeschke, Matthew D Robson, and Aaron T Hess. "Cardiac gating using scattering of an 8-channel parallel transmit coil at 7T". In: *Magnetic Resonance in Medicine* 80.2 (2018), pp. 633–640.

[13] Mette K Stam et al. “Navigators for motion detection during real-time MRI-guided radiotherapy”. In: *Physics in Medicine & Biology* 57.21 (2012), p. 6797.

[14] D.Buikman, T. Helzel, and Peter Röschmann. “THE RF-COIL AS A SENSITIVE MOTION DETECTOR FOR MRI STUDIES UP TO 2 TESLA”. In: Jan. 1986.

[15] Thomas Vahle et al. “Respiratory Motion Detection and Correction for MR Using the Pilot Tone: Applications for MR and Simultaneous PET/MR Examinations.” In: *Investigative Radiology* (2019).

[16] Mario Bacher. “Cardiac Triggering Based on Locally Generated Pilot-Tones in a Commercial MRI Scanner: A Feasibility Study”. PhD thesis. Graz University of Technology (90000), 2017.

[17] DA Seeber, J Jevtic, and A Menon. “Floating shield current suppression trap”. In: *Concepts in Magnetic Resonance Part B: Magnetic Resonance Engineering: An Educational Journal* 21.1 (2004), pp. 26–31.

[18] Marc Fischer et al. “Open-Sourced, Stereotax-Integrated, High-Fidelity and Adjustable 4-Channel Receive Array for Primate Brain Imaging at 3T”. In: *ISMRM Meeting and Exhibition Abstract* (2020). URL: https://archive.ismrm.org/2020/4036.html.

[19] Jana Delfino et al. “MRI-related FDA adverse event reports: A 10-yr review”. In: *Medical Physics* 46 (Aug. 2019). DOI: 10.1002/mp.13768.

[20] Laurent Giovangrandi et al. “Ballistocardiography – A Method Worth Revisiting”. In: *Conference proceedings : ... Annual International Conference of the IEEE Engineering in Medicine and Biology Society. IEEE Engineering in Medicine and Biology Society. Conference* 2011 (Aug. 2011), pp. 4279–82. DOI: 10.1109/IEMBS.2011.6091062.

[21] Yuji Iwadate et al. “Enhancement of Respiratory Navigator-Gated Three-Dimensional Spoiled Gradient-Recalled Echo Sequence with Variable Flip Angle Scheme”. In: *Magnetic resonance in medicine : official journal of the Society of Magnetic Resonance in Medicine / Society of Magnetic Resonance in Medicine* 72 (July 2014). DOI: 10.1002/mrm.24902.